Atmospheric Research 216 (2019) 186–206

Contents lists available at ScienceDirect

Atmospheric Research

journal homepage: www.elsevier.com/locate/atmosres

Potential of an EnKF Storm-Scale Data Assimilation System Over Sparse Observation Regions with Complex Orography

D.S. Carrió[a,*], V. Homar[a], D.M. Wheatley[b]

[a] Universitat de les Illes Balears, Physics Department, Carretera de Valldemossa km 7.5, 07122, Palma de Mallorca, Spain
[b] Cooperative Institute for Mesoscale Meteorological Studies, University of Oklahoma, NOAA/OAR/National Severe Storms Laboratory, Norman, OK, United States

ARTICLE INFO

Keywords:
Data assimilation
EnKF
Radar reflectivity
HyMeX
WRF-DART
Western mediterranean

ABSTRACT

High-impact weather events over sparse data regions with complex orography, such as the Mediterranean region, remain a challenge for numerical weather prediction. This study evaluates, for the first time, the ability of a multiscale ensemble-based data assimilation system to reproduce a heavy precipitation episode that occurred during the first Special Observation Period (SOP1) of the Hydrological cycle in the Mediterranean Experiment (HyMeX). During the Intense Observation Period (IOP13) from 14 to 15 October 2012, convective maritime activity associated with an advancing cold front affected coastal areas of southern France, Corsica and Italy. With the main objective of improving forecasts of this weather event, a data assimilation (DA) system using the Ensemble Kalman Filter (EnKF) algorithm is implemented. The potential impact of assimilating conventional in-situ observations (METAR, aircrafts, buoys and rawinsondes) and single-Doppler reflectivity data to improve numerical representation of growing convective maritime structures that will evolve towards coastal populated areas is evaluated. Results indicate that information provided by both observation sources contribute to initiation and subsequent evolution of convective structures not captured by the conventional runs. Notably, data assimilation experiments produce the best quantitative verification scores for the short range (6–8 h) forecasts of accumulated precipitation. Beyond 6–8 h, data assimilation experiments and those without data assimilation are indistinguishable. Sensitivity experiments, evaluating the impact of increasing the length of the radar data assimilation period, reveal the importance of assimilating high-frequency reflectivity data during a mid-term period (6 h approx.) to better depict deep convective structures initiated over the sea that evolve towards populated coastal areas.

1. Introduction

During the late summer and autumn populated coastal areas in the Mediterranean basin are frequently impacted by heavy precipitation events that can lead to flash floods (e.g., Romero et al. (2000); Mariotti et al. (2002); Delrieu et al. (2005); Duffourg (2010); Ricard et al. (2012); Llasat et al. (2013)), leaving serious socio-economic impacts (e.g., Guzzetti et al. (2005); Salvati et al. (2010)). These kind of events are often linked to deep convection from mid-latitude cyclones or the development of intense quasi-stationary convective systems (Ducrocq et al. (2008); Davolio et al. (2009); Bech et al. (2011); Buzzi et al. (2014)) which still remains a key challenge of numerical weather forecasts (Weisman et al. (2008); Ducrocq et al. (2008); Rotunno and Miglietta (2011); Bresson et al. (2012)). Uncertainties in the initial and boundary conditions together with the chaotic behavior associated to the non-linear atmospheric dynamical equations can be considered as the major obstacle to obtain skillful forecasts. Besides, problems related to parameterizations used to describe the physical processes involved in the boundary layer over complex terrain and the difficulty that numerical weather models have with the initiation, amplitude and location of convection, also contributes to the inaccuracy of heavy precipitation forecasts (Barthlott and Kirshbaum (2013); Burton et al. (2013); Hanley et al. (2015)).

The international Hydrological cycle in the Mediterranean Experiment (HyMeX, Drobinski et al. (2014); http://www.hymex.org) coordinates scientific efforts to better understand the Mediterranean water cycle, and specifically its associated high impact events. During the HyMeX program, several special observation periods gathered large amounts of unique observations that provide a database that allows to better understand the physical processes involved in the genesis and posterior development of such events. During the autumn of 2012, specifically from 5 September to 5 November, the first Special

* Corresponding author.
E-mail address: diego.carrio@uib.es (D.S. Carrió).

https://doi.org/10.1016/j.atmosres.2018.10.004
Received 3 April 2018; Received in revised form 6 September 2018; Accepted 8 October 2018
Available online 11 October 2018
0169-8095/

Observation Period (SOP1) took place focusing on the monitoring, modeling and analysis of heavy precipitation events, flash floods and orographic precipitation events mostly affecting the Mediterranean areas of Spain, Italy and France (Ducrocq et al., 2014). During SOP1 field campaign, 20 intensive observation periods (IOPs) were performed, 9 of them in Italy. The observations collected and the diagnosed analysis achieved from the IOP experiments have provided the basis for several studies that investigate in detail the physical mechanisms involved in heavy precipitation events (Barthlott et al., 2014; Ferretti et al., 2014; Manzato et al., 2015). Most of these high impact events were initiated and developed over large data-void regions such as the Mediterranean Sea, where analyzed fields have larger errors due to the inherent lack of observations. Currently, uncertainties associated with the initial conditions are considered one of the main sources of error in properly predicting the location and timing of potentially dangerous convective scale storms (Wu et al., 2013). Among the entire set of IOPs, some of them were characterized by the presence of a deep trough over the Thyrrenian sea or by a cyclogenetic area over the Gulf of Genoa (e.g., IOP13, IOP16c, IOP18). However, for this study, we were interested in weather events that initiated or developed mainly over the sea that subsequently moved towards coastal areas affecting populated regions. Between the above-mentioned IOPs, the IOP13 (14–15 October 2012) heavy precipitation event, associated with a cold front intrusion from southern France to central Italy, was the only one that fulfill this requirements. This frontal system took place mainly over the Mediterranean basin traveling eastwards favoring the development of convective systems. For this reason, IOP13 was selected to perform our numerical sensitivity simulations. The convective systems associated to the IOP13 were developed and became organized intermittently in different areas and times, leading to an additional difficulty generating skillful forecasts for this event.

During the last 40 years, a variety of different data assimilation (DA) methods (i.e., statistical procedures that combine observational data and first-guess model state) have emerged with the main objective of reducing the uncertainty associated with the representation of initial condition. The data assimilation algorithm used in this study is the ensemble Kalman filter (EnKF; Evensen (1994)), which is a Monte Carlo approximation to the Kalman filter (Kalman, 1960). One of the main characteristic of EnKF is the estimation of the flow-dependent background-error covariance, which allows to analyze both observed and unobserved fields through cross-correlations (Snyder and Zhang, 2003) derived from the ensemble, as opposed to the static ones used in most variational data assimilation schemes (Parrish and Derber, 1992; Courtier et al., 1994). Interestingly, ensembles initialized by an EnKF analysis produce less biased forecasts for intense rainfall episodes (Schumacher and Clark, 2014). Several studies have demonstrated the ability of EnKF for assimilating data from synoptic-scale to convective-scale (Evensen, 1997; Houtekamer and Mitchell, 1998; Anderson and Anderson, 1999; Hamill and Snyder, 2000; Whitaker and Hamill, 2002; Reichle et al., 2002; Snyder and Zhang, 2003; Dowell et al., 2004; Zhang et al., 2004;Hacker and Snyder, 2005; Tong and Xue, 2005; Fujita et al., 2007; Snook et al., 2011; Wheatley et al., 2012; Yussouf et al., 2013b; Carrió and Homar, 2016).

Overall, the above-mentioned DA EnKF studies deal with severe weather events (typically tornadic supercell thunderstorms, damaging windstorms and flash floods) taking place over flat terrain (e.g., USA great plains). One of the greatest advantages is that National Weather Services (NWSs) from United States provide an extensive well-covered observational network, including observations from conventional (such as METARs (Meteorological Aerodrome Report), mesonet, rawinsondes or aircrafts) and operational Weather Surveillance Radar-1988 Dopplers (WSR−88Ds) that are also quality controlled. Despite most real case studies ude background filed sextracted from global models, which have standard observations already assimilated to correct the environment, these studies confirm quantitatively the great importance of assimilating reflectivity and radial velocity observations from Doppler radars into meso- and storm-scale models to improve such servere weather forecasts. However, it is noteworthy that EnKF DA studies, as those aforementioned, have in general three main common features. First, the assimilation phase is typically started when convection is initiated. This is a critical disadvantage from a practical predictability point of view, because it requires an active event. The potential of improving the precursor environment that hosts the convective initiation is not studied in detail. Second, once the last assimilation cycle is finished, the typical lead time is only a few hours or even minutes ahead. Details on how the forecast initiated from the EnKF analysis behaves in the short-range (6-24 h) are not typically discussed. Third, severe weather events studied emerge from an isolated convective structure, such as supercells or mesoscale convective systems (MCSs), with negligible interactions with other active systems.

The present study discusses the potentail predictability of a multiscale DA EnKF system in improving the short-range forecast of the high impact IOP13 case event. Contrary to past studies, this heavy precipitation episode initiated over the sea, where a lack of in-situ observations is present, and was also influenced by high complex orography (e.g., Alps and Pyrenees). This event was associated with a cold front intrusion progressing over the sea. Embedded in the front, multiple convective systems emerged and dissipated while interacting among them. This configuration hampered the generation of an accurate short-range forecast. This work is devoted to investigate the ability of an EnKF system to produce an accurate pre-convective environment hours before the onset of deep convective activity over the sea, to improve the predictability of this event. In particular, we investigate the impact of assimilating a set of in-situ and radar observations.

The remainder of this paper is organized as follows: Section 2 introduces a brief description of the heavy precipitation event using the available observations. The multiscale ensemble design, the observation sets ingested in the data assimilation process, and the configuration of the EnKF system is highlighted in Section 3. Section 4 provides the description of the experimental set-up design used in this study. Results obtained from sensitivity experiments in the assimilation and forecast period and their quantitative verification using several statistical scores are discussed in Section 5. Finally, Section 6 provides a discussion of the main results obtained and also offers suggestions for future studies.

2. Overview of the IOP13 heavy precipitation event

During the first observation period of the international HyMeX (Hydrological cycle in the Mediterranean Experiment) project, a heavy precipitation event took place between 14 and 15 October 2012 (IOP13). This event initially produced intense precipitation over southern coastal areas of France, later affecting the northern and central parts of Italy (Fig. 1). On 15 October, the Italian rain gauge network registered an accumulated precipitation maximum of 60 mm/24 h in central Italy, 160 mm/24 h in northeastern Italy and 120 mm/24 h in Liguria and Tuscany. The synoptic situation was dominated by a cold front associated with a wide upper-level trough extending from northern France towards northern Spain (Ferretti et al., 2014). During the night of 14 October a cold front affected the Western Mediterranean region and during 15 October the system rapidly progressed from France to Italy, advecting low-level moisture towards the western coast of Italy. In the following hours of 15 October, a shallow secondary minimum pressure system developed (coupled with a potential vorticity anomaly aloft) in the Gulf of Genoa, and the associated frontal system moved towards the Tyrrhenian coast, producing moist air advection causing high instabilities and favoring deep moist convective activity. During the evening of 15 October, the low pressure system moved across the northern Italian peninsula, and the associated precipitation affected the Balkan area in the morning of 16 October. A complete overview of the synoptic situation and observational data collected from the IOP13 event can be found in Ferretti et al. (2014) and Barthlott and Davolio (2016).

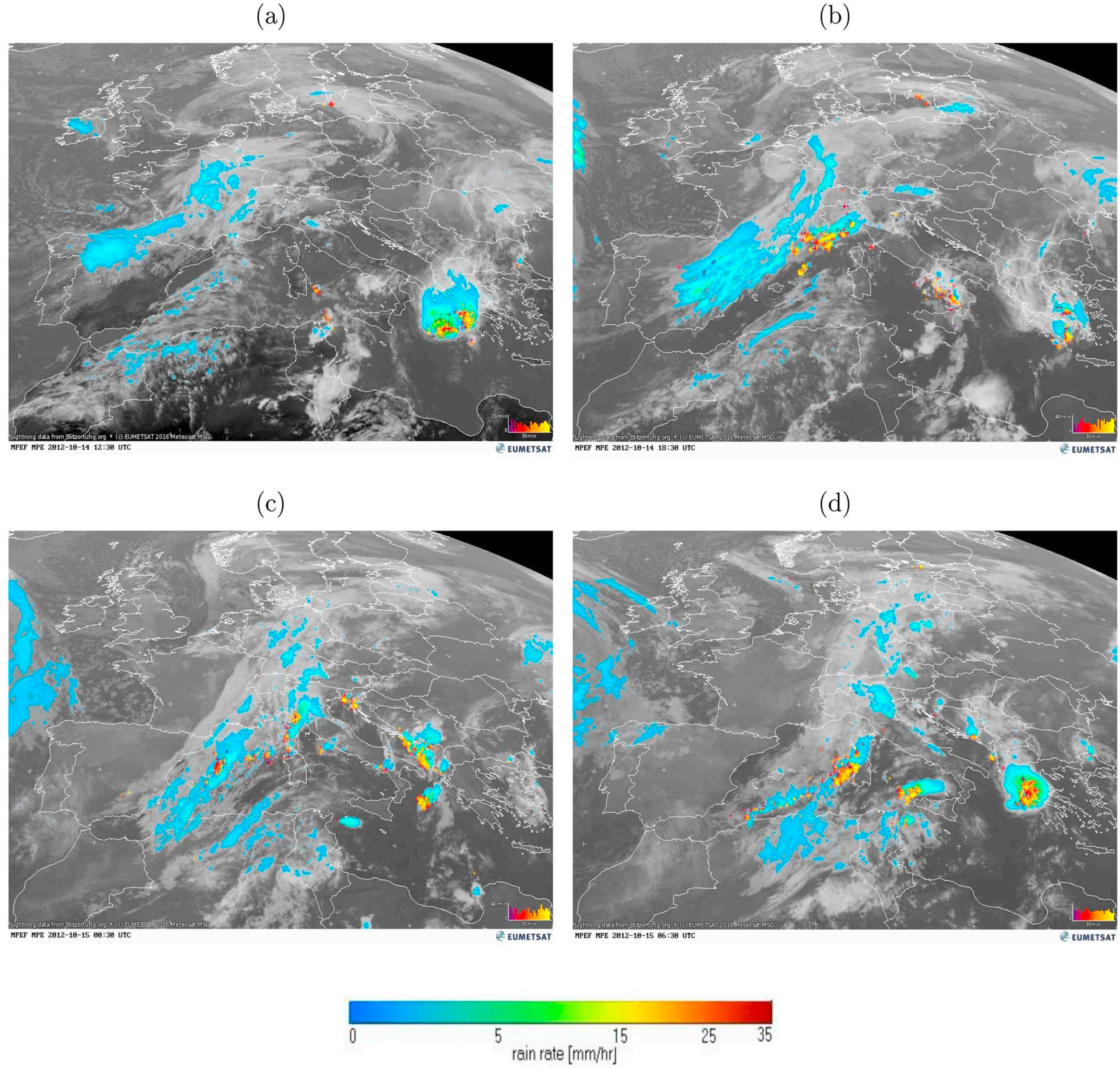

Fig. 1. EUMETSAT multi-sensor precipitation estimate combined with cloud coverage and lightning distribution depicting the synoptic situation over the Western Mediterranean region for: (a) 14 Oct 12 UTC, (b) 14 Oct 18 UTC, (c) 15 Oct 00 UTC and (d) 15 Oct 06 UTC.

3. Methodology

3.1. Multiscale WRF ensemble design

Given the great influence of meso- and storm-scale processes in the unfolding of the IOP13 impacts, a multiscale ensemble data assimilation system consisting of two nested domains similar to that used by Yussouf et al. (2015) is used. All experiments performed in this study make use of version 3.7 of the Advanced Research Weather Research and Forecasting Model (WRF-ARW; Skamarock et al., 2008). The parent domain is centered over the Western Mediterranean Sea, covering nearly the entire Europe and part of the northern Africa with a horizontal grid-point spacing of 15 km (Fig. 2). The nested storm-scale domain is centered over Genoa Gulf with a grid resolution of 3 km (Fig. 2). This configuration allows to simulate the easterly evolution of the cold front system and the associated convective structures that will produce the registered heavy precipitation events. The two numerical domains are featured with 51 vertical grid levels, from surface to the 50 hPa isobaric level. All numerical experiments are performed using 36-member ensembles, with boundary and initial conditions extracted from the European Center of Medium Range Weather Forecasts global Ensemble Predication System (EPS-ECMWF) at a horizontal and vertical spectral triangular truncation of T639 L62 (~31 km horizontal grid resolution). Despite these fileds are influenced by the routine data assimilation meso- and storm-scale data assimilation experiments (Isaksen et al., 2010; Bonavita et al., 2017). The EPS-ECMWF consists of 50 perturbed ensemble members plus a control ensemble member (50 + 1) using a horizontal and vertical spectral triangular truncation of T639 L62 (~31 km horizontal grid resolution). A Principal Components Analysis and k-mean clustering technique is used to select the 36

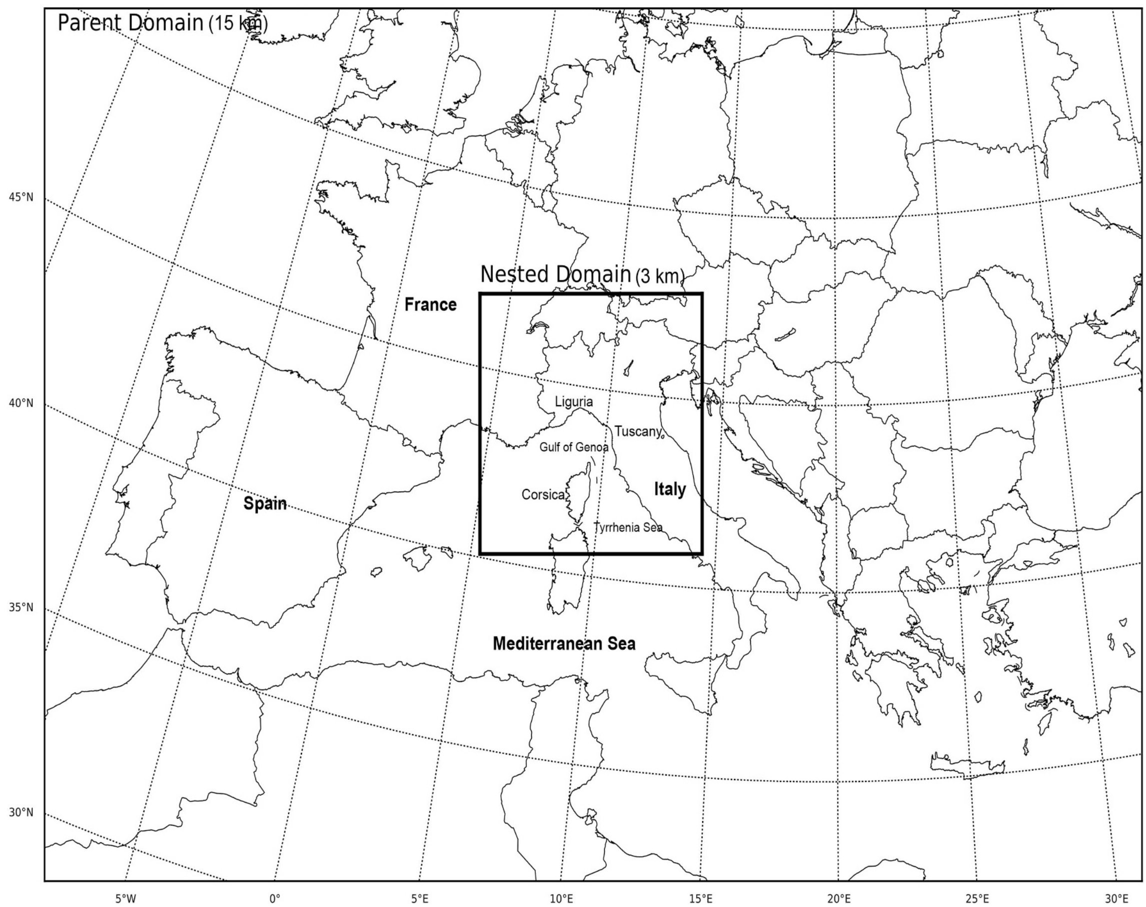

Fig. 2. Mesoscale and storm-scale domains used in all the numerical experiments.

ensemble members with the largest dispersion over the entire numerical domain (Garcies and Homar, 2009). To take into account the uncertainties in the numerical model (Stensrud et al. (2000); Fujita et al. (2007); Wheatley et al. (2012)), different combinations of physics parameterizations are used among the members (see Table 1). The diversity in the physics parameterizations include two shortwave (SW) and longwave (LW) radiation schemes [Dudhia (Dudhia, 1989) and RRTMG (Iacono et al., 2008)], three planetary boundary layer (PBL) schemes [Yonsei University (YSU; Hong et al., 2006), Mellor-Yamada-Janjić (MYJ; Janjić, 1990, 1996, 2002), and Mellor-Yamada-Nakanishi-Niino level 2.5 (MYNN2; Nakanishi and Niino, 2006, 2009)], and three cumulus parameterizations schemes [Kain-Fritsch (KF; Kain and Fritsch, 1993; Kain, 2004), Tiedtke (Tiedtke, 1989), and Grell-Freitas (GF; Grell and Freitas, 2013)]. The most relevant common physic options across the ensemble members are the microphysics and the land surface scheme. The Thompson microphysic (Thompson et al., 2004, 2008) and the Noah land surface scheme (Tewari et al., 2004) were used for this study. The parameterization schemes activated in the nested domain are identical to those in the parent domain except for the cumulus parameterization which is not required in the nested domain.

3.2. Observations

The NOAA's Meteorological Assimilation Data Ingest System (MADIS) provides a database of quality controlled[1] conventional data. Fig. 3 shows the spatial distribution of the set of observations containing altimeter pressure, dewpoint, temperature and horizontal winds from rawinsondes, buoys instruments, METARs and aircrafts that were assimilated in both meso- and storm-scale ensembles. In addition, reflectivity observations from Météo-France S-band Doppler radars were assimilated only in the storm-scale ensemble: ALERIA, located in the Corsica island (France) and NIMES located southern France (Fig. 8a). These data contain 5 and 9 scan angles respectively, with 5-min volume scan time, and they are available on the official website of HyMeX at https://www.hymex.org. With the main objective of avoiding issues related with signal aliasing and to decorrelate observation errors, these quality-controlled observations are objectively analyzed to a regularly spaced 6-km horizontal grid using the Cressman Interpolation algorithm (Wheatley et al., 2015; Yussouf et al., 2015). Reflectivity values below 0 dBZ are set to 0 dBZ and are considered to indicate "no precipitation". These preprocessed radar observations are assimilated every 15-min. Unfortunately, no quality controlled radial velocities are distributed from these radars, and thus the are not assimilated in this study.

To properly assimilate reflectivity observations, DART uses an observation operator that estimates reflectivity values from each ith hydrometeor class by a constant c_i multiplied by the 6th moment of the size distribution (Smith Jr et al., 1975; Lin et al., 1983; Smith, 1984; Schoenberg Ferrier, 1994; Gilmore et al., 2004; Caya, 2004):

$$Z_e \approx \sum_i c_i \int_0^\infty n_i(D) D^6 dD \tag{1}$$

where c_i is the radar calibration coefficient, $n_i(D)$ is the size distribution, and D is the particle diameter. The size distribution of the ith hydrometeor class is approximated by an exponential function:

$$n_i(D) = n_{0i} \exp(-\lambda_i D) \tag{2}$$

here, n_{0i} is the intercept parameter and λ is the slope parameter of the

[1] Using the technique described on-line at https://madis.ncep.noaa.gov/madis_qc.shtml

Table 1
Multi-physic parameterizations used on the WRF ensemble system presented on this study. Here PBL, SW and LW stand for planetary boundary layer, shortwave and longwave respectively.

Multiphysic configuration					
Ensemble members	Microphysics	Cumulus	PBL	Land Surface	SW/RW radiation
1	Thompson	KF	YSU	Noah	Dudhia
2		KF	YSU		RRTMG
3		KF	MYJ		Dudhia
4		KF	MYJ		RRTMG
5		KF	MYNN2		Dudhia
6		KF	MYNN2		RRTMG
7	Thompson	GF	YSU	Noah	Dudhia
8		GF	YSU		RRTMG
9		GF	MYJ		Dudhia
10		GF	MYJ		RRTMG
11		GF	MYNN2		Dudhia
12		GF	MYNN2		RRTMG
13	Thompson	Tiedke	YSU	Noah	Dudhia
14		Tiedke	YSU		RRTMG
15		Tiedke	MYJ		Dudhia
16		Tiedke	MYJ		RRTMG
17		Tiedke	MYNN2		Dudhia
18		KF	MYNN2		RRTMG
19	Thompson	KF	YSU	Noah	Dudhia
20		KF	YSU		RRTMG
21		KF	MYJ		Dudhia
22		KF	MYJ		RRTMG
23		KF	MYNN2		Dudhia
24		KF	MYNN2		RRTMG
25	Thompson	GF	YSU	Noah	Dudhia
26		GF	YSU		RRTMG
27		GF	MYJ		Dudhia
28		GF	MYJ		RRTMG
29		GF	MYNN2		Dudhia
30		GF	MYNN2		RRTMG
31	Thompson	Tiedke	YSU	Noah	Dudhia
32		Tiedke	YSU		RRTMG
33		Tiedke	MYJ		Dudhia
34		Tiedke	MYJ		RRTMG
35		Tiedke	MYNN2		Dudhia
36		Tiedke	MYNN2		RRTMG

size distribution. These parameters are related to the mixing ratio of the species q_i by the following expression:

$$\lambda_i = \left(\frac{\pi \rho_i n_{0i}}{\rho q_i}\right)^{0.25} \tag{3}$$

being ρ_i the density of the species and ρ the air density. Thus, the assimilation of reflectivity is associated with a mixture of hydrometeor types in the analysis, such as rain, dry and wet graupel/hail and dry and wet snow.

3.3. EnKF data assimilation system

In this study we use the parallel version of the Ensemble Kalman Filter (EnKF, Kalman (1960); Kalman and Bucy (1961); Burgers et al. (1998)) technique from the Trunk release branch (revision 9240) of the Data Assimilation Research Testbed software system (DART; Anderson and Collins (2007); Anderson et al. (2009)).

3.3.1. Mesoscale 1-h data assimilation

The MADIS conventional observations were ingested hourly from 00 UTC 14 October 2012 to 00 UTC 15 October 2012. This multiscale system runs using a one-way nested configuration with the parent domain providing boundary conditions for the inner domain. Each assimilation cycle, the EnKF updates the model state vector composed by the three dimensional prognostic fields of wind velocity, perturbation potential temperature, perturbation geopotential and perturbation surface pressure of dry air, as well as water vapor and the following hydrometeor fields: mixing ratio of cloud, rain, ice, snow, graupel and the number of concentration of rain and ice. It also updates some diagnostic fields such as 10-m wind fields, 2-m temperature and moisture, surface pressure and 10-cm reflectivity, which is useful to compute diagnostics on the assimilation results.

Covariances obtained from this modest ensemble size, which are the fundamental key of the EnKF algorithm, could suffer of significant misrepresentations due to the generation of spurious correlations, culminating in a poorer analysis (Hacker et al., 2007). The negative impact of sampling errors, is minimized by using a covariance localization technique (Houtekamer and Mitchell, 1998), which is based on a distance weighting function that goes to zero in distant region (Sobash and Stensrud, 2013). For this study we use a Gaussian localization function–the fifth-order piece-wise rational function of Gaspari and Cohn (1999)– to mitigate the negative effect due to the use of a limited ensemble system. A half-radius of 230 km in the horizontal and a half-radius of 4 km in the vertical are applied for the horizontal and vertical localizations.

The use of a moderate ensemble size is associated with a reduction in ensemble spread after each analysis cycle (Anderson and Anderson, 1999). To reduce this impact and help to maintain spread in the mesoscale system, an adaptive inflation is applied to the prior ensemble state for each assimilation cycle. In this study we use a mean initial inflation value of 1.0 with 0.6 of standard deviation. Further details on this procedure can be found in Anderson and Collins (2007) and Anderson et al. (2009).

An additional quality control method is performed by the filter algorithm where the difference between the observation and the prior ensemble mean exceeds 3 times the square root of the sum of the prior ensemble variance and the observation error variance. Observational errors used in this study are analogous to table 3 in Romine et al. (2013) with minor exceptions: METAR altimeter (1.5 hPa), marine altimeter (1.20 hPa) and METAR and marine temperature (1.75 K).

3.3.2. Storm-scale 15-min data assimilation

In order to better simulate the timing and intensity of the deep moist convective activity of IOP13, a storm-scale domain with 3 km horizontal grid resolution centered over Genoa is used. Reflectivity observations from Doppler radars, METAR, radiosonde, aircraft and buoys observations are assimilated every 15-min from 18 UTC 14 October 2012 to 00 UTC 15 October 2012. Radial velocities from Doppler radars have been demonstrated in past studies very useful to improve weather forecasts. However, these observations were not assimilated in the present study because they were not quality controlled and presented aliasing features together with a very noisy data. The task of performing an efficient quality control algorithm is beyond the scope of this study. Initial and boundary conditions for the storm-scale 15-min data assimilation system are obtained from the hourly updated largest mesoscale domain. The no-precipitation reflectivity observations are also assimilated into the system to help reduce spurious convective activity that develop in the numerical model (Tong and Xue, 2005; Dowell et al., 2011).

The horizontal and vertical half-radius covariance localization for reflectivity observations is set to 9 km and 3 km respectively. Additional spread in form of random local perturbations are added to each ensemble member's horizontal wind, temperature and water vapor where reflectivity exceed 25 dBZ, using an additive noise technique (Dowell and Wicker, 2009). This technique is applied once the model state is updated by the filter algorithm and just before the ensemble is evolved in time until the next assimilation cycle. The local perturbations have standard deviation of 0.5 m s^{-1} for horizontal winds and 0.5 K for dewpoint and temperature (Dowell et al., 2011; Yussouf et al., 2013a). For the storm-scale data assimilation, the quality control associated with the filter algorithm also excludes those observations which exceed the outlier threshold mentioned in the mesoscale data assimilation

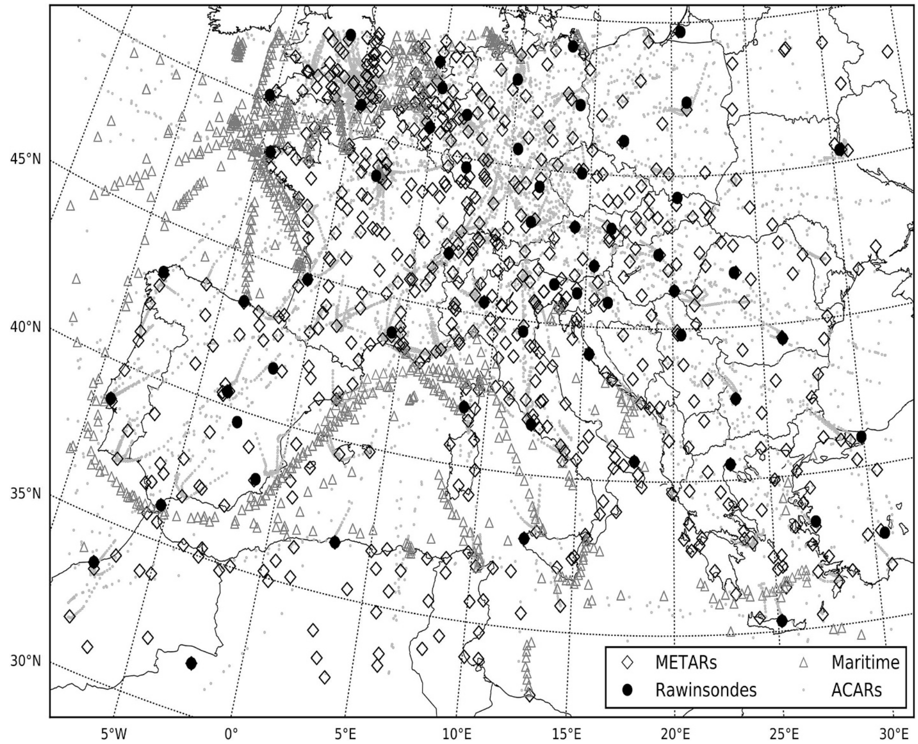

Fig. 3. Spatial distribution of conventional METARs, maritime buoys, rawinsondes and ACARs data assimilated on the multiscale system between 12 UTC on 14 Oct and 00 UTC on 15 Oct 2012.

section. For the reflectivity observations a standard deviation error of 5 dBZ was adopted, in line with following Wheatley et al. (2014) and Yussouf et al. (2015).

4. Experimental design

4.1. Numerical simulation configuration

With the main purpose of assessing the added value of assimilating conventional and Doppler radar observations in a storm-scale environment, three numerical experiments have been designed. In the first experiment (CNTRL), conventional and radar observations were assimilated. For the second experiment (SYN), only conventional observations were ingested into the system. Finally, in the third experiment (NODA), no observations were assimilated. The intercomparison between the experimental results will help quantify the impacts of each observation type over the simulations of the IOP13 heavy precipitation event.

4.1.1. CNTRL experiment

The CNTRL experiment is designed to investigate the impact of assimilating both in-situ conventional and radar observations. Two Doppler radar sites covering part of the maritime area provide observations during the time period of this simulation. The assimilation of these radar observations could contribute significantly to improve the forecasts of the initiation of convection over the sea, as well as to improve the storm representation of both analyzed and short-range forecast.

The experimental design consists of three phases. On the first phase, the initial sample which is obtained from the clustering technique applied to the EPS-ECMWF (Section 3.1), is initialized at 18 UTC 13 October 2012 and it is forecasted 6 h forward until 00 UTC 14 October 2012 to spin-up the storm-scale domain. Then, on the second phase, hourly conventional observations (METARs, rawinsondes, aircrafts and buoys) were assimilated from 00 UTC 14 October to 00 UTC 15 October 2012. A rapid-update assimilation cycle (15-min) was also performed adding reflectivity observations from 18 UTC 14 October to 00 UTC 15 October (Fig. 4 Ia). Finally, the last phase consists in advancing the ensemble analysis, obtained through the last data assimilation cycle at 00 UTC 15 October, 24-h forward until 00 UTC 16 October.

4.1.2. SYN experiment

This experiment assesses the impact of conventional observations, which are useful to characterize mesoscale atmospheric circulation signatures. The SYN experiment incorporates the same three phases that the CNTRL one, but with a slight variation in the second phase. SYN experiment only takes into account in-situ conventional observations, as no radar observations are incorporated. An hourly data assimilation cycle is performed from 00 UTC 14 October to 00 UTC 15 October 2012. Then, in the forecast step, the new analysis state is integrated 24-h forward (Fig. 4 Ib).

4.1.3. NODA experiment

Finally, an experiment with no data assimilation is run. This experiment is a direct downscaling from the initial sample, obtained from the EPS-ECMWF, from 00 UTC 15 October to 00 UTC 16 October 2012 (Fig. 4 Ic). The comparison between NODA, SYN and CNTRL will highlight on the impact of the observations in each DA experiment. The choice of 00 UTC 15 October as the initial time for NODA, which matches the initial time for the forecast phase of CNTRL and SYN, allows comparison of the predicted fields as well as the analysis from the DA experiments. It is important to highlight that the choice of starting the NODA experiment from the EPS-ECMWF at 00 UTC 15 October was made intentionally to be able to transfer the conclusions obtained into operational contexts. The main argument that supports the decision of using the 00 UTC 15 October EPS-ECMWF analysis is the rapid error growth at the mesoscale and microscale. The large error growth of a free forecast in a case of active dynamics and spread convective activity likely results in large forecast errors. In an operational framework, this advises to use the most recent global forecast cycle available, which at

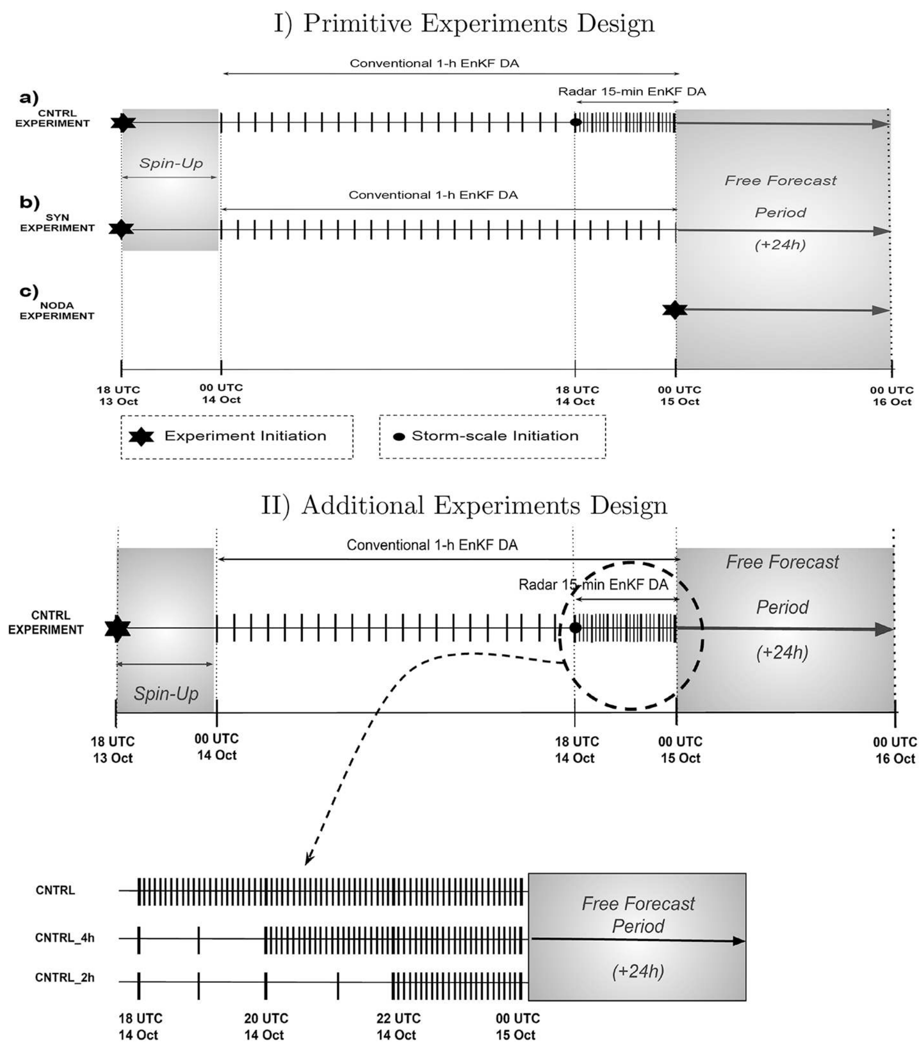

Fig. 4. Timeline of the different multiscale experimental designs employed in this study. Configuration in section I) corresponds to the primary experiments in this study a) CNTRL, b) SYN and c) NODA. Section II) corresponds to the experiments performed in the study of the impact of different DA period lengths in the numerical forecast. CNTRL experiment performs a 6-h cycle of reflectivity DA, CNTRL_4h experiment performs a 4-h period of DA and CNTRL_2h experiment performs only a cycle of 2-h of DA.

the time the DA analysis is produced is the 00 UTC 15 October.

4.2. Verification scores

To quantitatively evaluate the quality of the forecasts, several categorical and probabilistic verification scores have been used. As this study is focused on the improvement of a high precipitation event forecast, the verification is performed over the accumulated precipitation field (mm h^{-1}). Observational data registered by the Italian rain gauge network was used for this purpose.

One of the most widely used verification scores in the community to assess the forecast accuracy is the root mean squared error (RMSE). In this study, RMSE was computed for the accumulated precipitation fields from the three above-mentioned experiments.

The Brier score (BS; Wilks (2011)) is similar to the RMSE but for probabilistic forecasts of an event. The Brier score is negatively oriented, with perfect forecasts exhibiting BS = 0. The Brier skill score (BSS) is commonly used to compare the probabilistic forecast to a reference forecast (e.g., climatology). In this study, the NODA experiment is taken as the reference, leading to:

$$BSS = 1 - \frac{BS}{BS_{NODA}} \tag{4}$$

Hence, this score will indicate whether the CNTRL and SYN experiments improve upon the NODA experiment. Positive values of BSS imply an improvement with respect to the NODA experiment.

The relative operating characteristics (ROCs, Mason (1982); Stanski et al. (1989); Harvey Jr et al. (1992)) is considered a recommended method by the World Meteorological Organization for indicating the skill of a probabilistic weather forecasts. It compares the hit rate (warning provided correctly) against the false-alarm rate (warning provided incorrectly) for different probability thresholds. In the present study we applied the area under the relative operating characteristics (RAUCs, Stanski et al. (1989); Schwartz et al. (2010)) which is also a widely used method to assess the quality of the forecasts. Perfect forecasts render RAUC = 1.

Taylor diagrams (Taylor, 2001) are another way of proving graphical verification information. These diagrams display different patterns (experiment ensembles) in terms of their correlation, root mean squared error and amplitude of their variations (standard deviations). Taylor diagrams are useful tools to perform intercomparisons among multiple experiments, as those performed in this study.

5. Results

We discuss in this section the most relevant aspects of the

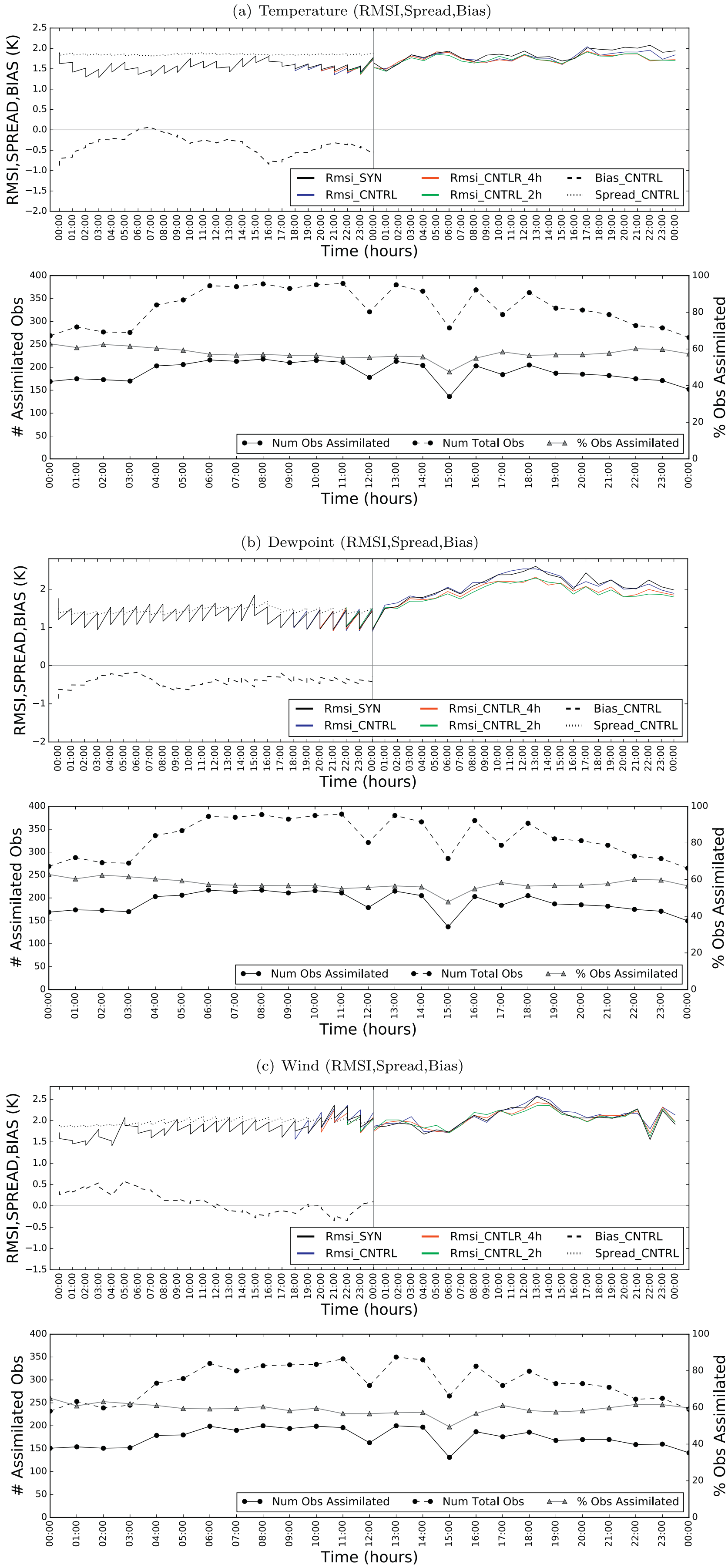

(caption on next page)

Fig. 5. Observation-space diagnostics for 1-h assimilated conventional data during a period of 24 h on the 14 October 2012. Values for RMSI, Bias and total spread for each DA experiments are depicted for (a) 2 m temperature, (b) 2 m dewpoint and (c) 10 m y-component of wind observations. RMSI for the forecast period is also added. For each these observations there are an additional panel showing the total number of available observations (dashed black lines), the number of assimilated observations (solid dark lines) and the percentage of assimilated observations (gray lines).

experiments performed. First, the ability of the EnKF algorithm to fit the model state to the observations is discussed. Second, a quantitative verification of the short-range forecast using the above-mentioned scores is performed with the main aim of estimating the impact of the initial conditions obtained in the previous assimilation step.

5.1. Observation-space diagnostics

With the primary purpose of checking that the assimilation process is performing as expected, observation-space diagnostic statistics of the root mean squared innovation (RMSI), total ensemble spread and bias are calculated (Dowell and Wicker, 2009; Dawson II et al., 2012; Yussouf et al., 2013b; Wheatley et al., 2014). The RMSI gives a measure of the overall fit of the forecasts and analysis to the observations and it can be defined as:

$$RMSI = \sqrt{<d^2>} \tag{5}$$

where $d = y^o - \overline{H(x)}$ is the innovation, defined as the difference between observations and the interpolated mean simulated values. H is the forward observational operator which converts the numerical model fields (in model-space) to the equivalent observed measures (in observation-space). H also performs the corresponding spatial interpolation which allows to compare the model and the observations point-wise. The angle brackets indicate expected value over all assimilated observations in order to quantify the impact of assimilating observations into the system, the RMSI is computed before (prior; x^f) and after (posterior; x^a) each analysis cycle. The second statistic measure is the total ensemble spread (TS) defined by Dowell and Wicker (2009) as:

$$TS = \sqrt{\sigma_{obs}^2 + < \frac{1}{N-1}\sum_{n=1}^{N}[H(x_n) - \overline{H(x)}]^2>} \tag{6}$$

where σ_{obs} is the observational standard deviation error assumed for each kind of assimilated observation and N is the ensemble size (i.e., 36). Alternatively, the bias highlights systematic errors associated with the ensemble performance. Analyses bias has been calculated through the mean innovation as Yussouf et al. (2015):

$$Bias = < -d> \tag{7}$$

The hourly conventional data ingested from 00 UTC 14 October to 00 UTC 15 October was firstly evaluated for every MADIS observation type by calculating the above-mentioned statistics prior- and posterior-to each analysis cycle, generating in this way a sawtooth-like pattern of these diagnostics. Prior and posterior RMSI values for the entire set of conventional observations range from ~0.5 to 1.5 (K, hPa or m s^{-1}) during the assimilation period (Fig. 5). Diagnostics from the 2-m temperature and the x-component of the wind show similar behavior with the dewpoint and y-component of the wind, respectively. These errors together with the spread show a slight growth in the early part of the assimilation due to the spin-up effect of the data assimilation system and afterwards they remain stable around the observational error, which is a sign of robustness and performance of the system.

RMSI was computed during the window assimilation (from 00 UTC 14 October to 00 UTC 15 October) for all DA experiments with the aim of showing the model error growth between assimilation steps corresponding to the different experiments (Fig. 5). In general, it can be shown that the inclusion of radar observations help reducing the RMSI through cross-correlations, although this effect is very sensitive to the meteorological fields. The RMSI for the 10-m wind is greater reduced when radar observations are assimilated than the RMSI for 2-m dewpoint or temperature. The 24-h forecast verification among the different DA experiments is also depicted in the same figure, showing that in general, the assimilation of reflectivity observations help to reduce the error of the above-mentioned variables (Fig. 5). It is also important to note that the forecast error growth after all DA cycles is similar to those during the DA cycles.

The consistency ratio (CR; Dowell et al. (2004)) diagnostic is used to assess the consistency between the prior ensemble spread and RMSI with the observation error:

$$CR = \frac{(TS)^2}{(RMSI)^2} = \frac{\sigma_{obs}^2 + < \frac{1}{N-1}\sum_{n=1}^{N}[H(x_n) - \overline{H(x)}]^2>}{<d^2>} \tag{8}$$

where the total spread and RMSI are calculated over the prior states.

Thus, a consistency ratio of ~1.0 suggests that the prior spread is a good approximation of the forecast error for the assumed observation error. Consistency ratios computed for the whole period of assimilation generally fall between 0.5 and 1.5 (Fig. 6). For altimeter observations, large values of consistency ratio are observed during the first hours of the assimilation window, gradually decreasing as the system assimilates new observations and until the last cycle of the assimilation window, where proper values of consistency ratio were reached (Fig. 6a).

Diagnostic statistics were also calculated to the rapid-update (15-min) storm-scale radar data assimilation (Fig. 7), for regions where reflectivity exceeds 20 dBZ. Initially, before the first reflectivity assimilation cycle, the RMSI depicts a large value of 22 dBZ, attributable to the lack of maritime convective systems identifiable on the radar fields. As the EnKF system cycles forward in time, these errors start decreasing and at the end of the assimilation window the RMSI reach approximately 3 dBZ (Fig. 7a). The BIAS is also corrected down to around 10 dBz, similar to Dong and Xue (2013). Such high innovations reveal the limited ability of the model to maintain the convective systems introduced by the assimilation filter. Analogous to the conventional statistics results, the total spread does not depict any collapse or divergence of the ensemble system, remaining stable most of the DA window indicating robustness of the data assimilation design. Consistency ratio for the reflectivity shows an initial growth during the spin-up period from 0.2 to 0.5, and then remain stable for the rest of the assimilation period (Fig. 7b). These consistency ratio values (< 1) indicate that the ensemble system is underdispersive for the reflectivity observations treated. In general, this property is a common issue in real data assimilation studies at these scales (Aksoy et al., 2009; Snook et al., 2011; Jung et al., 2012; Yussouf et al., 2013a; Wheatley et al., 2014).

5.2. Model-space diagnostics

A new set of initial conditions (analysis) were obtained at 00 UTC 15 October through the posterior ensemble obtained from the last data assimilation cycle. At this time, a qualitative evaluation of the reflectivity fields retrieved from each experiment with the observed reflectivity corresponding to ALERIA and NIMES radars (Fig. 8) was performed. CNTRL simulates a significant *meso* convective system (MCS) eastern Corsica Island (see S1 pattern in Fig. 8c-d) and over the

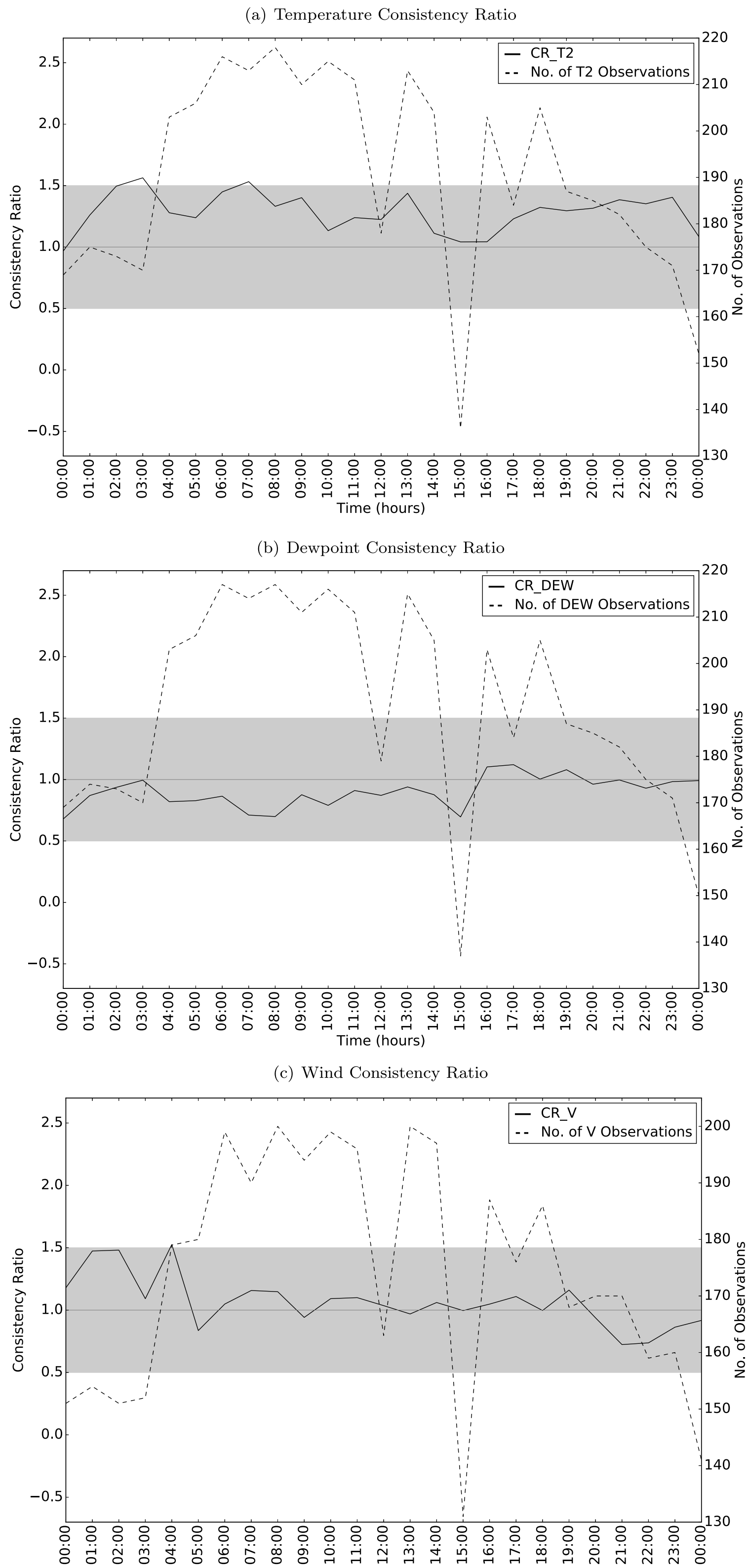

Fig. 6. Consistency ratios (solid lines) calculated using the prior ensemble mean during the whole period of conventional DA on the 14 October 2012. Number of assimilated observations (dashed lines) are also depicted. Gray areas indicate the range of consistency ratios closer to the perfect score (CR = 1).

Gulf of Genoa (see S2 pattern in Fig. 8c–d). A direct visual intercomparison against SYN shows that reflectivity assimilation also contributes in reducing the intensity of some convective structures offshore southern France and removing spurious convection generated by the model (see S3 and S4 patterns in Fig. 8b-d). On the other side, NODA (Fig. 4a) initially does not develop reflectivity structures because it is a cold start simulation, and some time is needed to allow the model to generate convective structures. Thus, the assimilation of conventional and radar observations allows to produce realistic convective structures at the correct location. However, the intensity of some of these simulated convective structures is overestimated compared to the observations (e.g., S2 pattern in Fig. 8c–d).

Conventional and radar data assimilation in the EnKF modify substantially the dynamical and thermodynamical environment

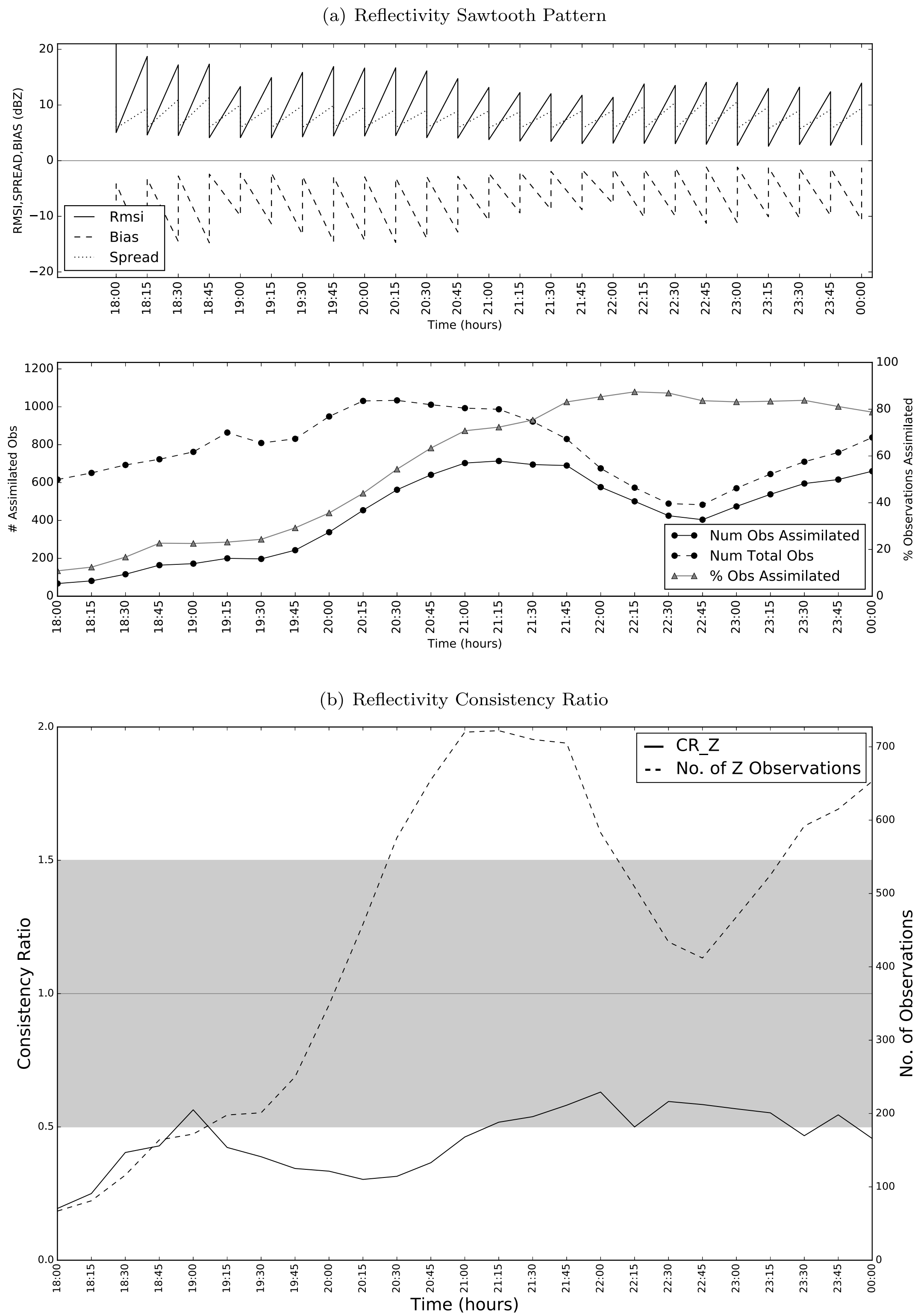

Fig. 7. As in Fig. 5 and Fig. 6, but for the 15-min radar data assimilation experiment from 18 UTC 14 October to 00 UTC 15 October 2012.

represented by the numerical model. For this case, the assimilation of such observations revealed a greater impact in the thermodynamic environment (characterized by the equivalent potential temperature) than in the dynamic fields. The impact in the thermodynamic environment linked to every type of observation assimilated, was analyzed using differences between the assimilation-experiments (CNTRL, SYN) and the no-assimilation experiment (NODA), or the differences between CNTRL and SYN experiments (Fig. 9). In the first instance, the impact of assimilating both conventional and radar reflectivity observations compared with the NODA experiment (Fig. 9b) is to warm the column of air (~ 12 K) located between 41.56°N/10.81°E and 41.15°N/11.31°E that is related with the latent heat release from the MCS (S1 in Fig. 8c) generated by the assimilation of reflectivity data. A secondary warming corresponding to a smaller convective cell over eastern Corsica island (Fig. 8c) is also present to the west of the above-mentioned main MCS. The second main effect of assimilating reflectivity data (CNTRL experiment) is the modification of the cold front system intrusion (westernmost part of the cross section). It can be showed that the assimilation of such observations cools down (~ −9 K) the cold front system which was the main triggering mechanism of convection of this event, and also it is moved forward to the east of the cross section. The impact of the assimilation from conventional observations (Fig. 9c), shows that the cold front cooling was mainly due to these observations. Finally, the comparison of the impact of assimilating reflectivity versus conventional data shows that the main impact of the reflectivity data in the thermodynamical environment is to warm up the column for the largest MCS and warming along the convective structure east of Corsica (Fig. 9d). Although the assimilation of observations significantly affects the thermodynamic environment,it is also important to highlight the effect on the dynamical field, represented by the wind field. The cross section of the wind shows how the assimilation of conventional observations increases the wind along the cold front, shifting the cold front system eastwards. Thus, the impact of conventional observations is mainly to cool the atmosphere and shift the cold front system eastwards.

A forecast initialized at 00 UTC 15 October was launched for each experiment and one of the most notable aspects found was that the MCS (S1 in Fig. 8c) developed eastern Corsica by the CNTRL simulation, gradually lost intensity while it was moving towards the Italian coast (Fig. 10). When this MCS arrived to the coast at 02 UTC 15 October, a

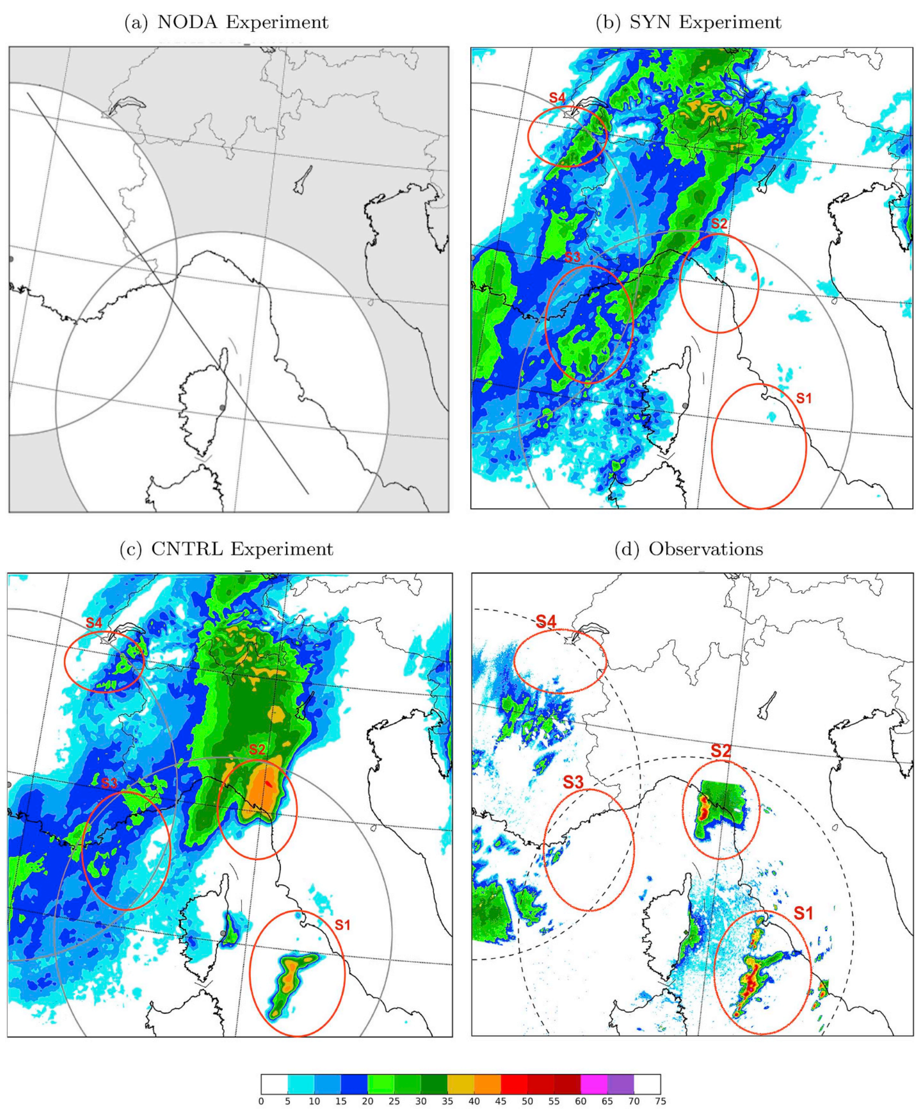

Fig. 8. Ensemble-mean reflectivity for (a) NODA, (b) SYN and (c) CNTRL experiments at analysis time (00 UTC 15 October 2012). The observed reflectivity field (d) at the same time is also shown. Gray dashed circumferences depicts the influence range of the radars. Red circles corresponds to areas of interest discussed in the manuscript. Gray line represents the location of a vertical cross section used along this study. (For interpretation of the references to colour in this figure legend, the reader is referred to the web version of this article.)

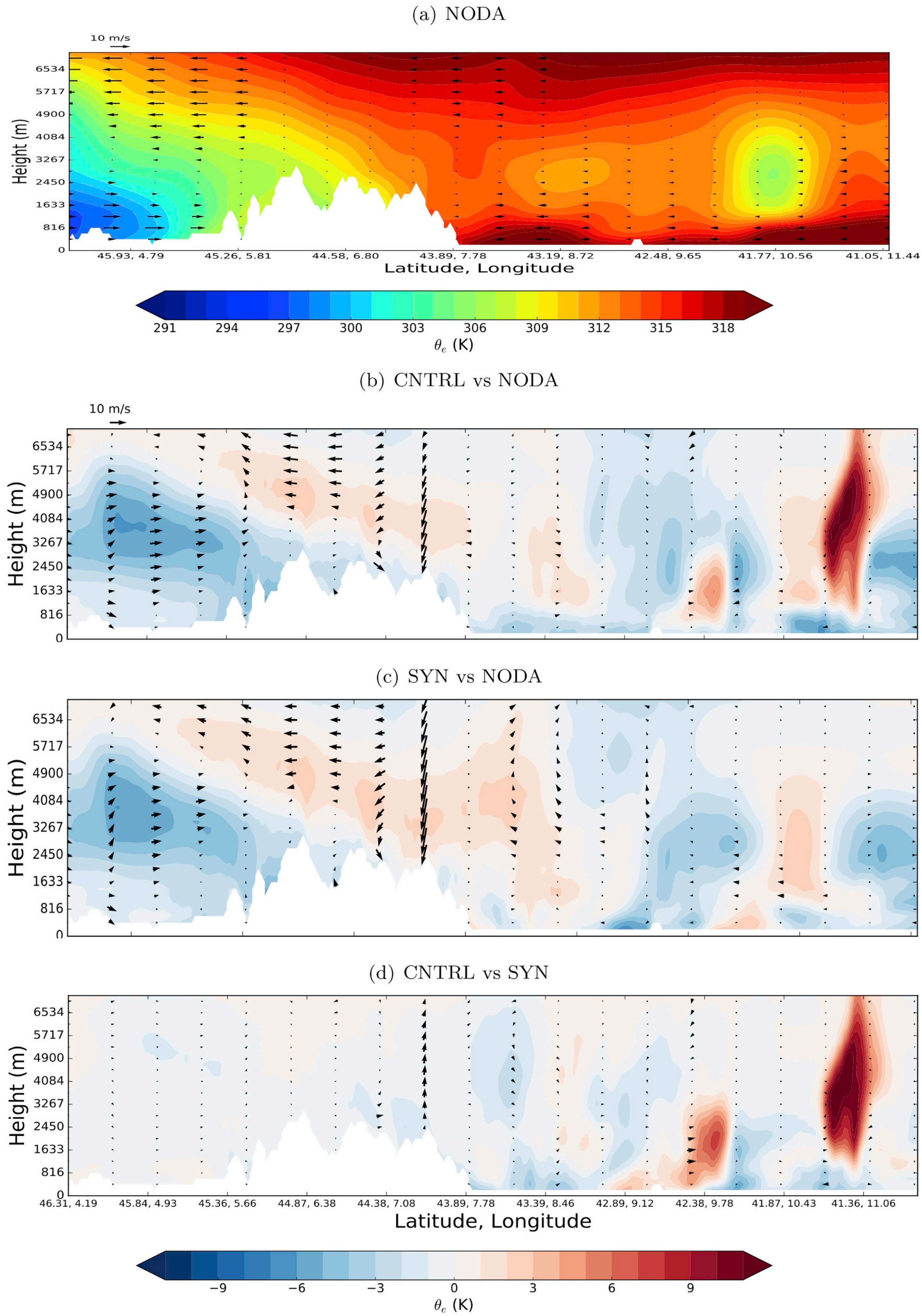

Fig. 9. Vertical cross section along the inner domain depicted in Fig. 8a, showing the ensemble mean equivalent potential temperature and wind for a) the NODA experiment and also for the differences between experiments b) CNTRL-NODA, c) SYN-NODA and d) CNTRL-SYN at the analysis time (00 UTC 15 October 2012).

mismatch between the shape and intensity of the system and the observations is clearly observed (Fig. 10c–d). At 04 UTC, the observed MCS still remained over the Italian coast while the CNTRL simulated reflectivity field does not produce any significant signal at the same location. Thus, deep convective structures inserted in the numerical model through reflectivity data assimilation rapidly decay within 4–6 h in the forecast. As time evolves, simulated convective systems in both SYN and CNTRL experiments become more similar to the NODA ones. Therefore, assimilating observations does not have significant effect after a few hours, in this case, after 6 h approximately. The inability of the forecast model to maintain structures generated by the assimilation filter is a well known limitation of EnKF systems, even under favourable circumstances such as the simulation of mostly isolated well-defined structures like cyclones, mesoscale convective systems or supercells (e.g., Fujita et al. (2007); Kain et al. (2010); Snook et al. (2011); Wheatley et al. (2012); Stensrud et al. (2013); Wheatley et al. (2015); Yussouf et al. (2016)). These studies typically are focused on isolated weather systems that rarely interact with other convective systems or complex geographical features. In addition, most storm-scale assimilation experiments in the literature benefit from using dense observational networks with excellent monitoring strategies that result in valuable quality controlled observational databases used in the assimilation process. For the present study, we highlight the potential of EnKF techniques in a region with lack of in-situ observations where most of them are located in high complex terrain. We also show the weaknesses of current observational systems, in the Mediterranean region, helping in the improvement of the predictability of severe weather events that produce high economical and social losses. Better regional initiatives to promote building quality observational databases would help overcome the challenges that the lack of observations and the complex geographical features pose to storm-scale data assimilation in the Mediterranean. In addition to the inherent model difficulty in maintaining the convective structures introduced by the data assimilation system, there is another predictability challenge associated with this kind of case study. This event was affected by multiple intermittent convective cells associated with the evolution of the cold front that swept the Italian peninsula during the late hours of 14 and the entire 15 October. The final analysis obtained from the EnKF contains information of active convection before the first hours of 15 October. In spite of the fact that conventional and radar assimilation also helps to improve the thermodynamical and dynamical environment is not enough to initiate new observed convection later on.

As it was mentioned in the introduction section, this event was characterized as a heavy precipitation episode. For this reason and with the major aim of studying the impact of assimilating the above-mentioned observations in the short range forecast, the 2-h accumulated precipitation was computed for each experiment (Fig. 11). The CNTRL simulation reveals a better agreement in the location of the maximum amount of 2 h accumulated precipitation, compared to SYN and NODA simulations, with the observations provided by the Italian raingauges close to the Genoa Gulf (see O1 in Fig. 11d). SYN experiment shows a maximum of 2 h accumulated precipitation over the Genoa Gulf but shifted northwestwards relative to the observations. In addition, the assimilation of reflectivity observations helps to reduce the amount of precipitation depicted by the SYN simulation in some areas of the numerical domain (e.g., O2 in Fig. 11b-c). At this time and due to its cold-start initiation, NODA simulation was influenced by the spin-up period depicting a precipitation field that does not correspond to the observations. At 06 UTC the NODA simulation depicts a maximum of 2 h accumulated precipitation close to the maximum observed in northern Italy but it is overestimated (see O3 and O5 in Fig. 11e,d). The assimilation of conventional and reflectivity observations improve the location and intensity of the 2 h accumulated precipitation forecast (Fig. 11g) and also improve some overestimated precipitation areas depicted by the SYN simulation (see O4 in Fig. 11f–d). Ten hours after the forecast initiation, CNTRL simulation still has the 2 h accumulated precipitation forecast that is closer to the observations than the SYN and NODA experiments (Fig. 11k). Although NODA simulation depicts with good accuracy the maximum amount of precipitation near the Genoa Gulf, (O6 in Fig. 11f–d), it under-performs the accumulated precipitation in O7. In addition, NODA simulation overestimates the precipitation amount in O8 and O9. By this time, the differences between SYN and CNTRL simulations are negligible.

To quantitatively assess the impact of data assimilation on the forecast, several categorical and probabilistic verification scores (introduced in Section 4.2) were used for the 2-h accumulated precipitation field (Fig. 12). First, we focused our attention at the very short range forecast (2–8 h). Over this short-range forecast period, the RMSE, BSS and RAUC scores for the CNTRL experiment indicate best skills, followed by the SYN and NODA experiments respectively. This score shows that CNTRL simulation has initially lower errors compared with SYN and NODA results, which depict similar RMSE along the entire forecast period (Fig. 12a). These results are in agreement with the differences discussed above for Fig. 11. During the first 10 h of forecast, CNTRL experiment still having the best scores in terms of RMSE, and then the scores from all three experiments evolve essentially together becoming indistinguishable until the end of the forecasts where the errors range from 4 to 5 mm.

To be able to quantify the results from our simulations in terms of the accuracy of their probabilistic forecasts, the BSS using a threshold of 10 mm and also using as reference the NODA experiment was computed (Fig. 12b). The BSS indicates that the CNTRL probabilistic forecast (bounded to this threshold) exhibits a strong positive impact from the assimilation of both radar reflectivity and conventional observations during the first 8–10 h. On the other hand, SYN results show a negative impact of the conventional observations assimilation, contrary what one may expect from results depicted in Fig. 11a–d. However, Fig. 11b, shows hat the maximum accumulated precipitation pattern simulated in the Genoa Gulf is shifted from the observations towards the northwest of Italy, producing false alarms that penalize the forecast skill in terms of BSS. After 10 h of the initiation of the forecast, BSS shows similar behaviors for both CNTRL and SYN experiments. By this time the assimilation of conventional and reflectivity observations does not have a positive effect compared with the NODA simulation. The area under the ROC curve is also computed to evaluate the results obtained in terms of probabilistic forecasts (Fig. 12c). Again, CNTRL experiment depicts the best verification scores within the first hours of simulation, with values compressed between 0.84 and 0.86, reaffirming that the assimilation of conventional and reflectivity observations improve the short-range forecasts (Snook et al., 2015; Bick et al., 2016).

Finally, to complete our attempt to quantitatively measure the skill of our experiments in terms of 2-h accumulated precipitation, the Taylor diagram (Fig. 13) was computed at 02, 04 and 06 UTC 15 October. This diagram allows to analyze the accuracy of the ensemble members, quantifying the correspondence with the observations in terms of: Pearson correlation, RMSE and standard deviation. Results at 02 UTC show that ensemble members from the CNTRL simulation are characterized to have the highest correlation values (0.6–0.8) and lowest RMSE compared to the SYN and NODA experiments (Fig. 13a). Regarding the spread of the ensemble, the CNTRL ensemble depicts the largest standard deviations ranging from 2.4 to 5.7 mm, indicating that the assimilation of both conventional and reflectivity observations introduces extra variability to the ensemble. At this time, the NODA experiment has the worst performance, with correlation ranging from 0.2 to 0.4 and standard deviations values for all the ensemble members below the mean value associated with the observations. As the forecasts advanced in time the three different ensemble clusters (NODA, SYN and CNTRL) converge, becoming almost indistinguishable.

5.3. Sensitivity on the reflectivity DA period length

Reflectivity assimilation window in the CNTRL simulation was set up to 6 h performing assimilation cycles every 15-min. With the main

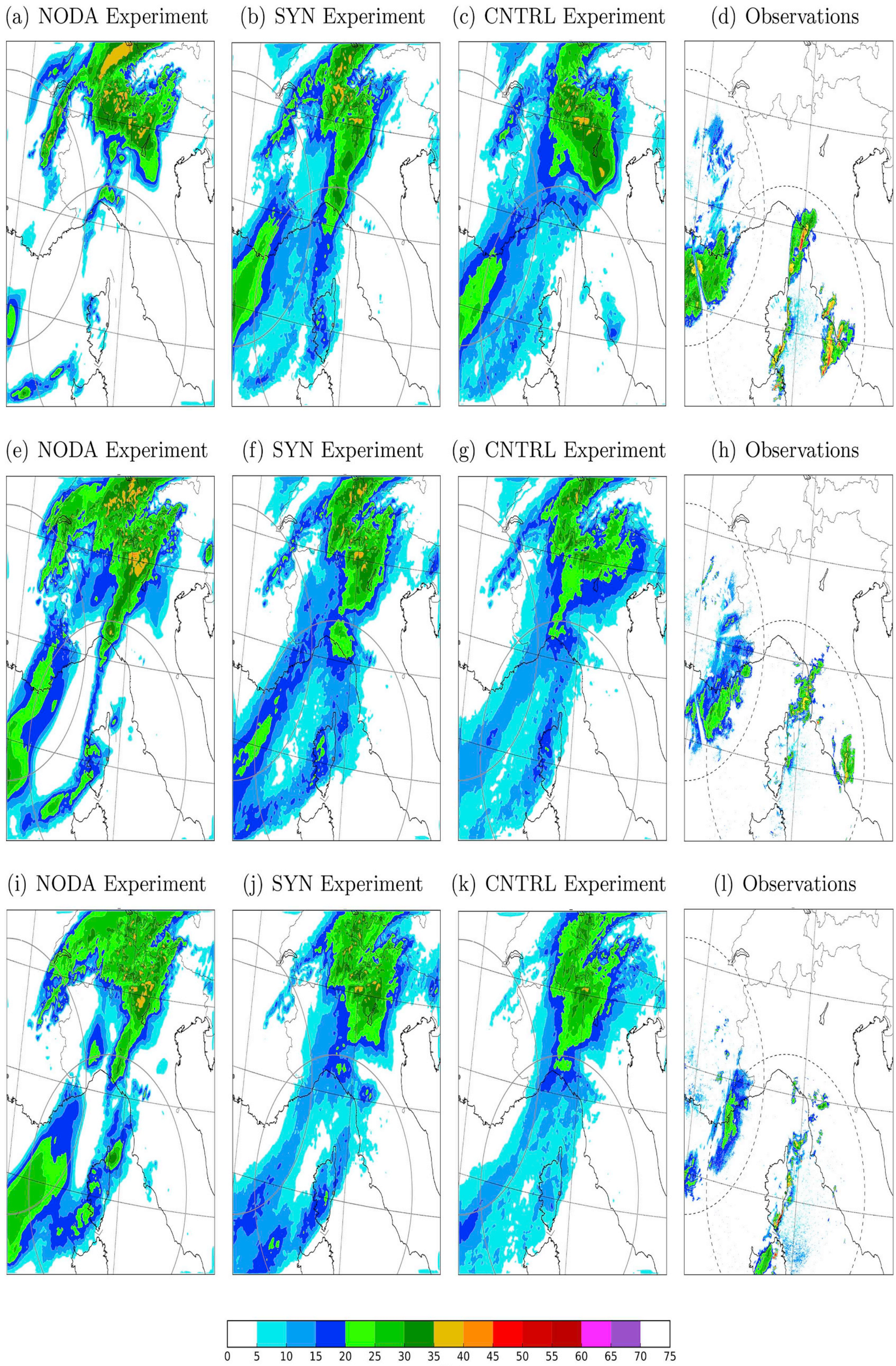

Fig. 10. Ensemble-mean reflectivity for NODA, SYN, CNTRL experiments and the associated reflectivity observations at 02 UTC (a,b,c,d), 04 UTC (e,f,g,h) and 06 UTC (i,j,k,l) on 15 October 2012.

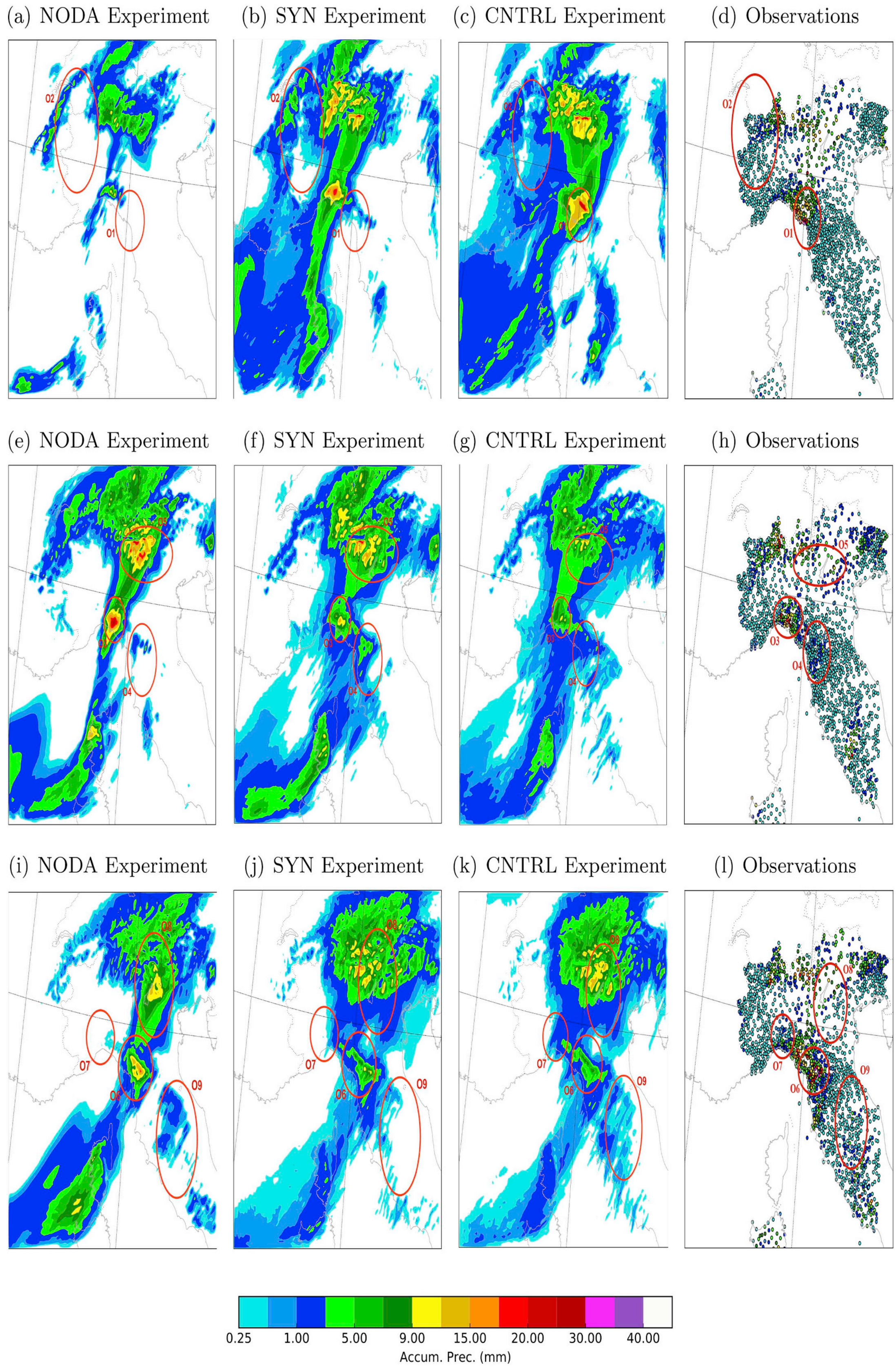

Fig. 11. Ensemble-mean 2-h accumulated precipitation for NODA, SYN, CNTRL experiments and the associated 2-h accumulated precipitation estimates from raingauges observations valids at 02 UTC (a,b,c,d), 06 UTC (e,f,g,h) and 10 UTC (i,j,k,l) on 15 October 2012.

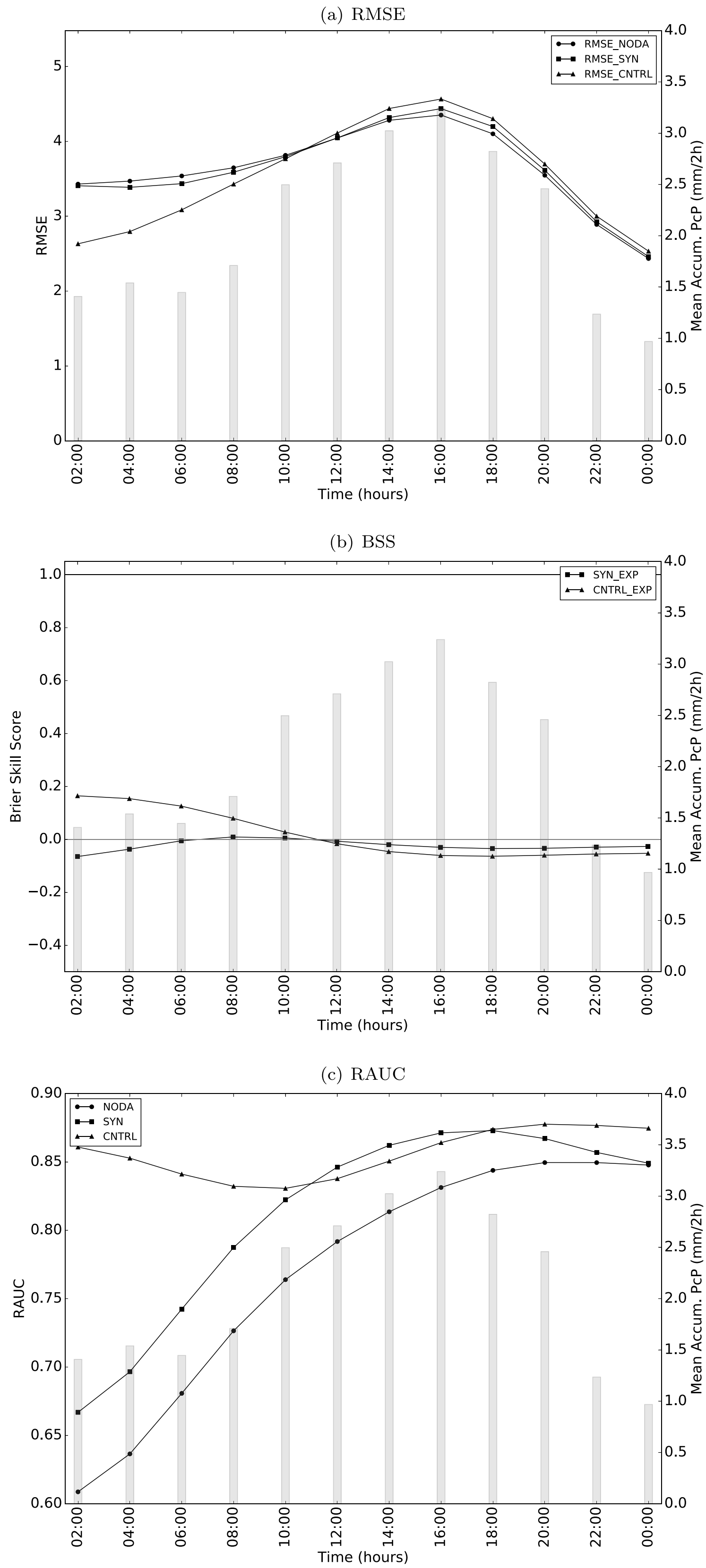

Fig. 12. Statistical verification scores a) RMSE, b) BSS and c) RAUC used for the forecast verification of the 2-h accumulated precipitation during 15 October over the Italian region within the inner domain of simulation.

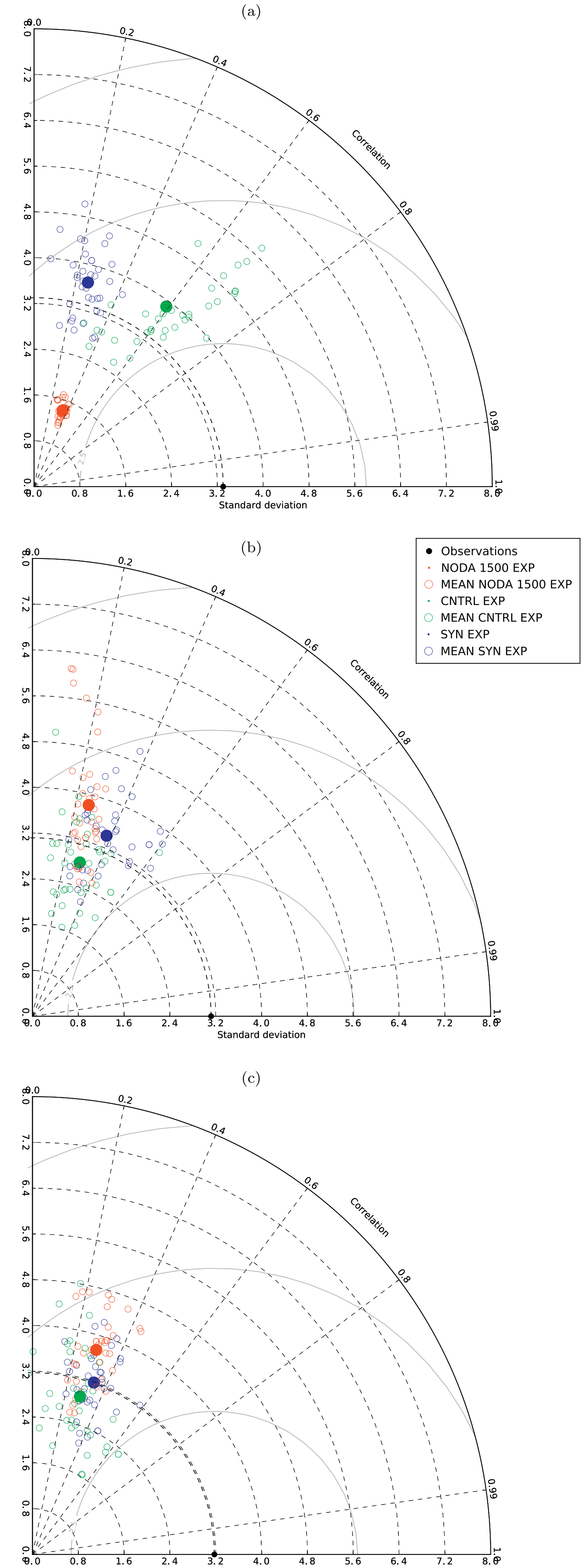

Fig. 13. Taylor diagrams performed by the CNTRL (green points), SYN (blue points) and NODA experiments (red points) for the 2-h accumulated precipitation valid at a) 02 UTC, b) 04 UTC and c) 06 UTC on 15 October 2012. (For interpretation of the references to colour in this figure legend, the reader is referred to the web version of this article.)

purpose of quantitatively assess the impact of the assimilation window length on the short-range forecast, two additional experiments were performed. Although the assimilation period was modified it still having the same assimilation frequency (see Fig. 4 II). On the one hand, the CNTRL_4h experiment assimilates reflectivity observations during 4 h, from 20 UTC 14 October to 00 UTC 15 October. And in the other hand, CNTRL_2h experiment only assimilates observations during 2 h, from 22 UTC 14 October to 00 UTC 15 October.

The analysis in the CNTRL_2h at 00 UTC 15 October reveals that the 2-h accumulated precipitation field missed in locating the maximum amount of observed precipitation, shifted northwards. This simulation results also show signs of underestimation in the amount of precipitation near the Genoa Gulf and northern Italy in comparison with the raingauges observations. However, when the assimilation window is elongated with two additional hours (CNTRL_4h), errors in the location of the maximum amount of precipitation and the underestimation values in some areas of the numerical domain are reduced significantly. These uncertainties in the CNTRL_2h and CNTRL_4h experiments are related with a poor representation of the northern part of the cold front system, covered by NIMES radar. This fact reveals the key role of NIMES radar in improving the depiction of the atmosphere state and the corresponding forecast. To evaluate quantitatively this effect from the probabilistic point of view, RAUC statistics are performed (Fig. 14). Results over the 2-h accumulated precipitation field confirm that CNTRL_2h gives the worst RAUC score, followed by the CNTRL_4h experiment indicating the relevance of the duration of the reflectivity assimilation period. These results agree with Dong and Xue (2013) regarding the importance of assimilating reflectivity observations during assimilation window periods longer than 2 h to obtain accurate forecasts using the EnKF system. In addition, RMSI for the assimilation and forecast periods are also depicted together with the other DA experiments, showing that CNTRL_4h and CNTRL_2h are indistinguishable verifying over 2-m temperature, dewpoint and 10-m wind (Fig. 5). However, more studies with similar features (such as, lack of observations, development of the thunderstorm over the sea and influence of complex orography) need to be performed to confirm these conclusions.

6. Synthesis and conclusions

During 14 and 15 October 2012, the HyMeX IOP13 heavy precipitation event advanced from southern coastal areas of France and towards central and northern populated areas of Italy. This event was associated with the intrusion of a cold front system that evolved mainly over the Western Mediterranean sea favoring intermittent mesoscale convective systems to develop that moved eastwards hitting the coastal area of Italy.

One of the most relevant source of uncertainties in numerical weather prediction is related with the predictability of first kind (Mu et al., 2002). This work aims to explore, for the first time, the ability of a multiscale EnKF DA to improve the predictability of severe weather events initiated over large maritime areas affected by high complex topography, such as the Mediterranean basin, where a lack of in-situ observations is present. Under such data sparsity observations available in these regions cannot be quality controlled at the same level as the operational network used in USA National Prediction Centers and poses a serious challenge to the prediction of Mediterranean severe weather events initiated over the sea. With the main objective of improving the representation of the atmosphere state and thus improving the short-range numerical forecasts of this maritime event, several multiscale numerical data assimilation experiments using the EnKF algorithm

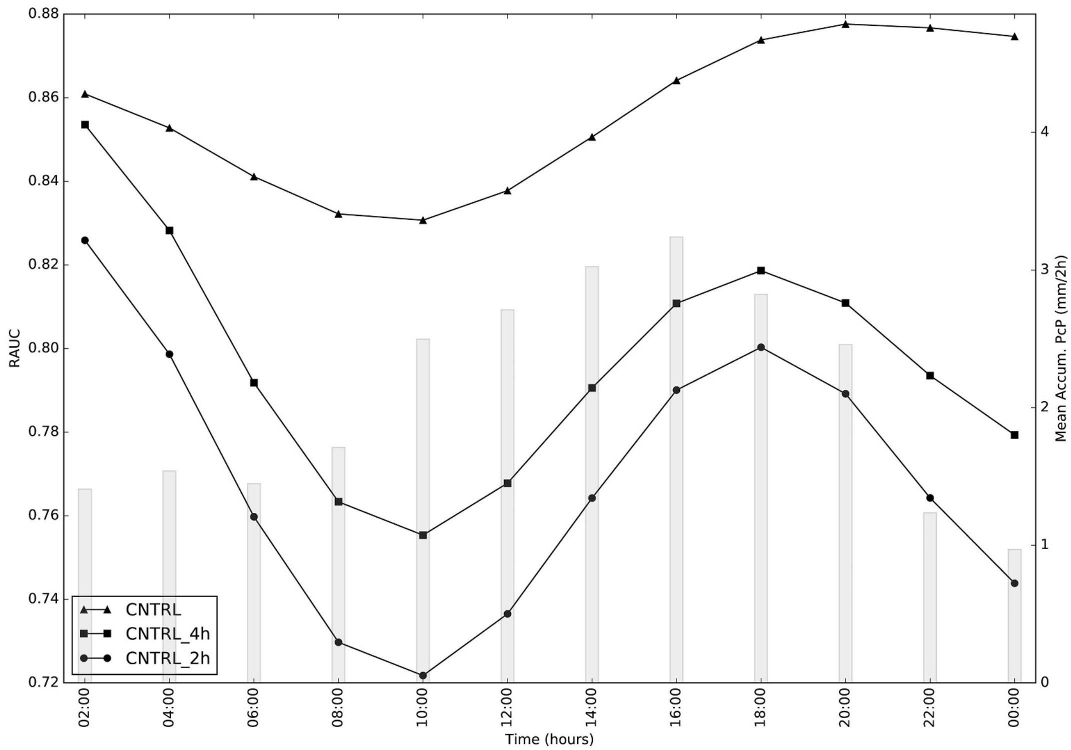

Fig. 14. As in Fig. 12 c, but for the sensitivity experiments: CNTRL (triangle marker), CNTRL_2h (dot marker) and CNTRL_4h (square marker).

were performed. The impact of assimilating in-situ conventional observations (ACARs, rawinsondes, METARs and maritime buoys) from MADIS database was evaluated. The impact of assimilating such observations (SYN) could be significant due to the advection of important synoptic/mesoscale features from coastal areas towards the sea by the assimilation cycle. Reflectivity data from two radars, one located southern France (NIMES) and the other in Corsica Island (ALERIA), together with the conventional observations were also assimilated (CNTRL). The spatial radar range of these radars covers a significant part of the sea where the cold front was located and provides information about active convective cells, that moved towards the Italian coast. To assess the quality of the underlying analysis fields, a numerical simulation without assimilating any kind of observations was also performed (NODA).

Results from these numerical experiments revealed that accumulated precipitation fields from CNTRL run (over the first 8–10 h of the simulation) were closer to the raingauge observations than the SYN and NODA experiments. Close inspection of the simulated reflectivity fields indicates that CNTRL simulation reproduced more precisely the observations of the mesoscale convective system over the sea, producing precipitation that SYN and NODA experiments did not simulate. The assimilation of conventional and reflectivity data also modified the dynamical and thermodynamical environments. Equivalent potential temperatures showed that the intensity and position of the cold front was modified (intensifying and moving forward such system) mainly by the conventional data assimilation effect. In contrast, reflectivity data assimilation had the major impact in warming the portion of the atmosphere associated with the development of deep convection.

To quantitatively assess the accuracy of each numerical experiment, several verification scores, such as RMSE, RAUC, BSS and Taylor diagrams, were computed. These scores indicate that the assimilation of both conventional and reflectivity observations have a major impact on the forecast, achieving the best verification scores among the other experiments during the first 10 h. Another important feature to highlight is the behavior of the forecasts for the CNTRL, SYN and NODA experiments after the first 8–10 h from the final analysis at 00 UTC. The forecasts of the three experiments basically converge after 10 h and they become essentially indistinguishable. Hence, the assimilation of radar and conventional observations does not have a significant impact beyond 10 h of free forecast. This is likely due to both the diurnal cycle minimum and the effects from our lateral boundary conditions from the large scale model.

Finally, we investigated the impact of the data assimilation window length on the CNTRL experiment. Two experiments were performed reducing the reflectivity window length from 6 to 4 and 2 h. Results showed that a 2-h window period was not enough to accurately represent the state of the atmosphere, mainly because during such short time period, the model can not represent sufficiently the convective structures responsible for the reflectivity intended to be assimilated.

In this study, the assimilation of high-resolution reflectivity observations have shown a great impact on the short-range forecast of maritime originated intermittent deep convective cells. However, a few number of radar instruments are located near coastal areas and they only cover a relative small area of maritime surface. For this reason, to further study the impact of assimilating observations to high impact weather initiated and developed over the sea, the assimilation of observations retrieved from meteorological instruments on board satellites is left for future studies. Among the available satellite products, we are interested in rapid-scan atmospheric motion vectors (RS-AMVs), which provide wind vector estimates over areas not covered by other observation means. These observations will be assimilated every 20 min together with conventional observations. The aim of this current research is to assess the impact of RS-AMVs on the predictability of maritime severe weather events.

Acknowledgements

This research is framed within the CGL2017-82868-R [Severe Weather Phenomena in Coastal Regions: Predictability Challenges and Climatic Analysis (COASTEPS)] and CGL2014-52199R [Future Regional Impacts of Climate Change Associated to Extreme Weather Phenomena (EXTREMO)] Spanish project which is partially supported with AEI/FEDER funds. The first author was also supported by the FPI-

CAIB (FPI/1877/2016) grant from the Conselleria d'Innovació, Recerca i Turisme del Govern de les Illes Balears and the Fons Social Europeu. The authors thankfully acknowledge Meteo-France for supplying the data and HyMeX database teams (ESPRI/IPSL and SEDOO/OMP) for their help in accessing the data. The authors also acknowledge the computer resources at MareNostrum IV and the technical support provided by Barcelona Supercomputing Center (RES-AECT-2017-1-0014, RES-AECT-2017-2-0014) that allowed us to perform the high-resolution simulations presented in this study. Thanks to Dr. Louis Wicker from the National Severe Storm Laboratory for his very useful comments on the manuscript and also thanks to Kent Knopfmeier for his technical assistance implementing the EnKF system.

References

Aksoy, A., Dowell, D., Snyder, C., 2009. A multicase comparative assessment of the ensemble kalman filter for assimilation of radar observations. part i: Storm-scale analyses. Mon. Wea. Rev. 137 (6).
Anderson, J.L., Anderson, S.L., 1999. A monte carlo implementation of the nonlinear filtering problem to produce ensemble assimilations and forecasts. Mon. Weather Rev. 127 (12), 2741–2758.
Anderson, J.L., Collins, N., 2007. Scalable implementations of ensemble filter algorithms for data assimilation. J. Atmos. Ocean. Technol. 24 (8), 1452–1463.
Anderson, J., Hoar, T., Raeder, K., Liu, H., Collins, N., Torn, R., Avellano, A., 2009. The data assimilation research testbed: A community facility. Bull. Am. Meteor. Soc. 90 (9).
Barthlott, C., Davolio, S., 2016. Mechanisms initiating heavy precipitation over italy during hymex special observation period 1: a numerical case study using two mesoscale models. Q. J. R. Meteorol. Soc. 142 (S1), 238–258.
Barthlott, C., Kirshbaum, D.J., 2013. Sensitivity of deep convection to terrain forcing over mediterranean islands. Q. J. R. Meteorol. Soc. 139 (676), 1762–1779.
Barthlott, C., Adler, B., Kalthoff, N., Handwerker, J., Kohler, M., Wieser, A., 2014. The role of Corsica in initiating nocturnal offshore convection. Q. J. R. Meteorol. Soc. 142 (S1), 222–237.
Bech, J., Pineda, N., Rigo, T., Aran, M., Amaro, J., Gayà, M., Arús, J., Montanyà, J., van der Velde, O., 2011. A mediterranean nocturnal heavy rainfall and tornadic event. Part i: overview, damage survey and radar analysis. Atmos. Res. 100 (4), 621–637.
Bick, T., Simmer, C., Tromel, S., Wapler, K., Hendricks Franssen, H.-J., Stephan, K., Blahak, U., Schraff, C., Reich, H., Zeng, Y., et al., 2016. Assimilation of 3d radar reectivities with an ensemble kalman filter on the convective scale. Q. J. R. Meteorol. Soc. 142 (696), 1490–1504.
Bonavita, M., Trémolet, Y., Holm, E., Lang, S.T.K., Chrust, M., Janisková, M., Lopez, P., Laloyaux, P., Rosnay, P.D., Fisher, M., Hamrud, M., English, S., 2017. A Strategy for Data Assimilation. ECMWF Tech Memo 800 (April).
Bresson, E., Ducrocq, V., Nuissier, O., Ricard, D., de Saint-Aubin, C., 2012. Idealized numerical simulations of quasi-stationary convective systems over the northwestern mediterranean complex terrain. Q. J. R. Meteorol. Soc. 138 (668), 1751–1763.
Burgers, G., Jan Van Leeuwen, P., Evensen, G., 1998. Analysis scheme in the ensemble Kalman filter. Mon. Wea. Rev. 126 (6).
Burton, R.R., Gadian, A., Blyth, A., Mobbs, S., 2013. Modelling isolated deep convection: A case study from cops. Meteorol. Z. 22 (4), 433–443.
Buzzi, A., Davolio, S., Malguzzi, P., Drofa, O., Mastrangelo, D., 2014. Heavy rainfall episodes over liguria in autumn 2011: numerical forecasting experiments. Nat. Hazards Earth Syst. Sci. 14 (5), 1325.
Carrió, D., Homar, V., 2016. Potential of sequential enkf for the short-range prediction of a maritime severe weather event. Atmos. Res. 178, 426–444.
Caya, A., 2004. Radar Observations in DART. DART Subversion repository.
Courtier, P., Thépaut, J.-N., Hollingsworth, A., 1994. A strategy for operational implementation of 4d-var, using an incremental approach. Q. J. R. Meteorol. Soc. 120 (519), 1367–1387.
Davolio, S., Mastrangelo, D., Miglietta, M., Drofa, O., Buzzi, A., Malguzzi, P., 2009. High resolution simulations of a flash flood near venice. Nat. Hazards Earth Syst. Sci. 9 (5), 1671–1678.
Dawson II, D.T., Wicker, L.J., Mansell, E.R., Tanamachi, R.L., 2012. Impact of the environmental low-level wind profile on ensemble forecasts of the 4 may 2007 greensburg, kansas, tornadic storm and associated mesocyclones. Mon. Weather Rev. 140 (2), 696–716.
Delrieu, G., Nicol, J., Yates, E., Kirstetter, P.-E., Creutin, J.-D., Anquetin, S., Obled, C., Saulnier, G.-M., Ducrocq, V., Gaume, E., et al., 2005. The catastrophic flash-flood event of 8–9 september 2002 in the gard region, france: a first case study for the cévennes–vivarais mediterranean hydrometeorological observatory. J. Hydrometeorol. 6 (1), 34–52.
Dong, J., Xue, M., 2013. Assimilation of radial velocity and reectivity data from coastal wsr-88d radars using an ensemble kalman filter for the analysis and forecast of landfalling hurricane ike (2008). Q. J. R. Meteorol. Soc. 139 (671), 467–487.
Dowell, D.C., Wicker, L.J., 2009. Additive noise for storm-scale ensemble data assimilation. J. Atmos. Ocean. Technol. 26 (5), 911–927.
Dowell, D.C., Zhang, F., Wicker, L.J., Snyder, C., Crook, N.A., 2004. Wind and temperature retrievals in the 17 May 1981 Arcadia, Oklahoma, supercell: Ensemble Kalman Filter experiments. Mon. Wea. Rev. 132 (8).
Dowell, D.C., Wicker, L.J., Snyder, C., 2011. Ensemble kalman filter assimilation of radar observations of the 8 may 2003 oklahoma city supercell: Inuences of reectivity observations on storm-scale analyses. Mon. Weather Rev. 139 (1), 272–294.
Drobinski, P., Ducrocq, V., Alpert, P., Anagnostou, E., Béranger, K., Borga, M., Braud, I., Chanzy, A., Davolio, S., Delrieu, G., et al., 2014. Hymex: A 10-year multidisciplinary program on the mediterranean water cycle. Bull. Am. Meteorol. Soc. 95 (7), 1063–1082.
Ducrocq, V., Nuissier, O., Ricard, D., Lebeaupin, C., Thouvenin, T., 2008. A numerical study of three catastrophic precipitating events over southern France. II: mesoscale triggering and stationarity factors. Q. J. Roy. Meteor. Soc. 134 (630).
Ducrocq, V., Braud, I., Davolio, S., Ferretti, R., Flamant, C., Jansa, A., Kalthoff, N., Richard, E., Taupier-Letage, I., Ayral, P.-A., et al., 2014. Hymex-sop1: the field campaign dedicated to heavy precipitation and flash flooding in the northwestern mediterranean. Bull. Am. Meteorol. Soc. 95 (7), 1083–1100.
Dudhia, J., 1989. Numerical study of convection observed during the winter monsoon experiment using a mesoscale two-dimensional model. J. Atmos. Sci. 46 (20), 3077–3107.
Duffourg, F., 2010. Sources et transports d'humidité pour les événements de pluies intenses en region méditerranéenne: caractérisation et assimilation à mésoéchelle de radiances satellitaires infrarouges. Université Paul Sabatier-Toulouse III (Ph.D. thesis).
Evensen, G., 1994. Sequential data assimilation with a nonlinear quasi-geostrophic model using Monte Carlo methods to forecast error statistics. JGR Oceans 99 (C5).
Evensen, G., 1997. Advanced data assimilation for strongly nonlinear dynamics. Mon. Weather Rev. 125 (6), 1342–1354.
Ferretti, R., Pichelli, E., Gentile, S., Maiello, I., Cimini, D., Davolio, S., Miglietta, M., Panegrossi, G., Baldini, L., Pasi, F., et al., 2014. Overview of the first hymex special observation period over italy: observations and model results. Hydrol. Earth Syst. Sci. 18 (5), 1953.
Fujita, T., Stensrud, D.J., Dowell, D.C., 2007. Surface data assimilation using an ensemble Kalman filter approach with initial condition and model physics uncertainties. Mon. Wea. Rev. 135 (5).
Garcies, L., Homar, V., 2009. Ensemble sensitivities of the real atmosphere: application to Mediterranean intense cyclones. Tellus 61 (3).
Gaspari, G., Cohn, S.E., 1999. Construction of correlation functions in two and three dimensions. Q. J. Roy. Meteor. Soc. 125 (554).
Gilmore, M.S., Straka, J.M., Rasmussen, E.N., 2004. Precipitation uncertainty due to variations in precipitation particle parameters within a simple microphysics scheme. Mon. Weather Rev. 132 (11), 2610–2627.
Grell, G.A., Freitas, S.R., 2013. A scale and aerosol aware stochastic convective parameterization for weather and air quality modeling. Atmos. Chem. Phys. Discuss. 13 (9).
Guzzetti, F., Stark, C.P., Salvati, P., 2005. Evaluation of flood and landslide risk to the population of Italy. Environ. Manag. 36 (1), 15–36.
Hacker, J.P., Snyder, C., 2005. Ensemble kalman filter assimilation of fixed screen-height observations in a parameterized pbl. Mon. Weather Rev. 133 (11), 3260–3275.
Hacker, J.P., Anderson, J.L., Pagowski, M., 2007. Improved vertical covariance estimates for ensemble-filter assimilation of near-surface observations. Mon. Wea. Rev. 135 (3).
Hamill, T.M., Snyder, C., 2000. A hybrid ensemble kalman filter–3d variational analysis scheme. Mon. Weather Rev. 128 (8), 2905–2919.
Hanley, K.E., Plant, R.S., Stein, T.H., Hogan, R.J., Nicol, J.C., Lean, H.W., Halliwell, C., Clark, P.A., 2015. Mixing-length controls on high-resolution simulations of convective storms. Q. J. R. Meteorol. Soc. 141 (686), 272–284.
Harvey Jr., L.O., Hammond, K.R., Lusk, C.M., Mross, E.F., 1992. The application of signal detection theory to weather forecasting behavior. Mon. Weather Rev. 120 (5), 863–883.
Hong, S.-Y., Noh, Y., Dudhia, J., 2006. A new vertical diffusion package with an explicit treatment of entrainment processes. Mon. Wea. Rev. 134 (9).
Houtekamer, P.L., Mitchell, H.L., 1998. Data assimilation using an ensemble Kalman filter technique. Mon. Wea. Rev. 126 (3).
Iacono, M.J., Delamere, J.S., Mlawer, E.J., Shephard, M.W., Clough, S.A., Collins, W.D., 2008. Radiative forcing by long-lived greenhouse gases: calculations with the aer radiative transfer models. J. Geophys. Res. 113 (D13).
Isaksen, L., Bonavita, M., Buizza, R., Fisher, M., Haseler, J., Leutbecher, M., Raynaud, L., 2010. Ensemble of data assimilations at ECMWF. European Centre for Medium-Range Weather Forecasts.
Janjić, Z.I., 1990. The step-mountain coordinate: Physical package. Mon. Wea. Rev. 118, 1429–1443.
Janjić, Z.I., 1996. The surface layer in the NCEP Eta Model. In: Preprints, 11th Conf. on Numerical Weather Prediction. Amer. Meteor. Soc, Norfolk, VA, pp. 354–355.
Janjić, Z.I., 2002. Nonsingular implementation of the Mellor-Yamada level 2.5 scheme in the NCEP Meso model. NCEP Office Note 437. (61 pp.).
Jung, Y., Xue, M., Tong, M., 2012. Ensemble kalman filter analyses of the 29–30 may 2004 oklahoma tornadic thunderstorm using one-and two-moment bulk microphysics schemes, with verification against polarimetric radar data. Mon. Weather Rev. 140 (5), 1457–1475.
Kain, J.S., 2004. The kain-fritsch convective parameterization: an update. J. Appl. Meteorol. 43 (1).
Kain, J.S., Fritsch, J.M., 1993. Convective parameterization for mesoscale models: The kain-fritsch scheme. In: The Representation of Cumulus Convection in Numerical Models. Springer, pp. 165–170.
Kain, J.S., Xue, M., Coniglio, M.C., Weiss, S.J., Kong, F., Jensen, T.L., Brown, B.G., Gao, J., Brewster, K., Thomas, K.W., et al., 2010. Assessing advances in the assimilation of radar data and other mesoscale observations within a collaborative forecasting–research environment. Weather Forecast. 25 (5), 1510–1521.
Kalman, R.E., 1960. A new approach to linear filtering and prediction problems. J. Fluid Eng. 82 (1).

Kalman, R.E., Bucy, R.S., 1961. New results in linear filtering and prediction theory. J. Fluid Eng. 83 (1).
Lin, Y.-L., Farley, R.D., Orville, H.D., 1983. Bulk parameterization of the snow field in a cloud model. J. Clim. Appl. Meteorol. 22 (6), 1065–1092.
Llasat, M., Llasat-Botija, M., Petrucci, O., Pasqua, A., Rosselló, J., Vinet, F., Boissier, L., 2013. Towards a database on societal impact of mediterranean floods within the framework of the hymex project. Nat. Hazards Earth Syst. Sci. 13 (5), 1337.
Manzato, A., Davolio, S., Miglietta, M.M., Pucillo, A., Setvák, M., 2015. 12 september 2012: a supercell outbreak in ne italy? Atmos. Res. 153, 98–118.
Mariotti, A., Struglia, M.V., Zeng, N., Lau, K., 2002. The hydrological cycle in the Mediterranean region and implications for the water budget of the mediterranean sea. J. Clim. 15 (13), 1674–1690.
Mason, I., 1982. A model for assessment of weather forecasts. Aust. Meteor. Mag 30 (4), 291–303.
Mu, M., Wansuo, D., Jiacheng, W., Mar 2002. The predictability problems in numerical weather and climate prediction. Adv. Atmos. Sci. 19 (2), 191–204. https://doi.org/10.1007/s00376-002-0016-x.
Nakanishi, M., Niino, H., 2006. An improved mellor–yamada level-3 model: Its numerical stability and application to a regional prediction of advection fog. Bound.-Layer Meteorol. 119 (2), 397–407.
Nakanishi, M., Niino, H., 2009. Development of an improved turbulence closure model for the atmospheric boundary layer. J. Meteorol. Soc. Jpn. Ser. II 87 (5), 895–912.
Parrish, D.F., Derber, J.C., 1992. The national meteorological center's spectral statistical-interpolation analysis system. Mon. Weather Rev. 120 (8), 1747–1763.
Reichle, R.H., McLaughlin, D.B., Entekhabi, D., 2002. Hydrologic data assimilation with the ensemble kalman filter. Mon. Weather Rev. 130 (1), 103–114.
Ricard, D., Ducrocq, V., Auger, L., 2012. A climatology of the mesoscale environment associated with heavily precipitating events over a northwestern mediterranean area. J. Appl. Meteorol. Climatol. 51 (3), 468–488.
Romero, R., Doswell III, C., Ramis, C., 2000. Mesoscale numerical study of two cases of long-lived quasi stationary convective systems over eastern Spain. Mon. Weather Rev. 128 (11), 3731–3751.
Romine, G.S., Schwartz, C.S., Snyder, C., Anderson, J.L., Weisman, M.L., 2013. Model bias in a continuously cycled assimilation system and its inuence on convection-permitting forecasts. Mon. Weather Rev. 141 (4), 1263–1284.
Rotunno, R., Miglietta, M., 2011. Application of theory to simulations of observed cases of orographically forced convective rainfall. Mon. Weather Rev. 140 (9), 3039–3053.
Salvati, P., Bianchi, C., Rossi, M., Guzzetti, F., 2010. Societal landslide and flood risk in italy. Nat. Hazards Earth Syst. Sci. 10 (3), 465–483.
Schoenberg Ferrier, B., 1994. A double-moment multiple-phase four-class bulk ice scheme. part I: description. J. Atmos. Sci. 51 (2), 249–280.
Schumacher, R.S., Clark, A.J., 2014. Evaluation of ensemble configurations for the analysis and prediction of heavy-rain-producing mesoscale convective systems. Mon. Weather Rev. 142 (11), 4108–4138.
Schwartz, C.S., Kain, J.S., Weiss, S.J., Xue, M., Bright, D.R., Kong, F., Thomas, K.W., Levit, J.J., Coniglio, M.C., Wandishin, M.S., 2010. Toward improved convection-allowing ensembles: model physics sensitivities and optimizing probabilistic guidance with small ensemble membership. Weather Forecast. 25 (1).
Skamarock, W., Klemp, J., Dudhia, J., Gill, D., Barker, D., Duda, M., Huang, X., Wang, W., Powers, J., 2008. A Description of the Advanced Research wrf Version 3, ncar Technical Note, Mesoscale and Microscale Meteorology Division. National Center for Atmospheric Research, Boulder, Colorado, USA.
Smith, P.L., 1984. Equivalent radar reectivity factors for snow and ice particles. J. Clim. Appl. Meteorol. 23 (8), 1258–1260.
Smith Jr., P., Myers, C., Orville, H., 1975. Radar reectivity factor calculations in numerical cloud models using bulk parameterization of precipitation. J. Appl. Meteorol. 14 (6), 1156–1165.
Snook, N., Xue, M., Jung, Y., 2011. Analysis of a tornadic mesoscale convective vortex based on ensemble kalman filter assimilation of casa x-band and wsr-88d radar data. Mon. Weather Rev. 139 (11), 3446–3468.
Snook, N., Xue, M., Jung, Y., 2015. Multiscale enkf assimilation of radar and conventional observations and ensemble forecasting for a tornadic mesoscale convective system. Mon. Weather Rev. 143 (4), 1035–1057.
Snyder, C., Zhang, F., 2003. Assimilation of Simulated Doppler Radar Observations with an Ensemble Kalman Filter*. Mon. Wea. Rev. 131 (8).
Sobash, R.A., Stensrud, D.J., 2013. The impact of covariance localization for radar data on EnKF analyses of a developing MCS: Observing system simulation experiments. Mon. Wea. Rev. 141 (11).
Stanski, H.R., Wilson, L.J., Burrows, W.R., 1989. Survey of common verification methods in meteorology. (World Meteorological Organization Geneva).
Stensrud, D.J., Bao, J.-W., Warner, T.T., 2000. Using initial condition and model physics perturbations in short-range ensemble simulations of mesoscale convective systems. Mon. Wea. Rev. 128 (7).
Stensrud, D.J., Wicker, L.J., Xue II, D.T.D., Yussouf, N., Wheatley, D.M., Thompson, T.E., Snook, N.A., Smith, T.M., Schenkman, A.D., Potvin, C.K., Mansell, E.R., Lei, T., Kuhlman, K.M., Jung, Y., Jones, T.A., Gao, J., Coniglio, M.C., Brooks, H.E., Brewster, K.A., 2013. Progress and challenges with warn-on-forecast. In: Atmos. Res. 123, 6th European Conference on Severe Storms 2011. Palma de Mallorca, Spain.
Taylor, K.E., 2001. Summarizing multiple aspects of model performance in a single diagram. J. Geophys. Res. 106 (D7), 7183–7192.
Tewari, M., Chen, F., Wang, W., Dudhia, J., LeMone, M., Mitchell, K., Ek, M., Gayno, G., Wegiel, J., Cuenca, R., 2004. Implementation and verification of the unified noah land surface model in the wrf model. In: 20th Conference on Weather Analysis and Forecasting/16th Conference On Numerical Weather Prediction. Vol. 1115.
Thompson, G., Rasmussen, R.M., Manning, K., 2004. Explicit forecasts of winter precipitation using an improved bulk microphysics scheme. part i: Description and sensitivity analysis. Mon. Weather Rev. 132 (2), 519–542.
Thompson, G., Field, P.R., Rasmussen, R.M., Hall, W.D., 2008. Explicit forecasts of winter precipitation using an improved bulk microphysics scheme. part ii: Implementation of a new snow parameterization. Mon. Weather Rev. 136 (12), 5095–5115.
Tiedtke, M., 1989. A comprehensive mass ux scheme for cumulus parameterization in large-scale models. Mon. Weather Rev. 117 (8), 1779–1800.
Tong, M., Xue, M., 2005. Ensemble kalman filter assimilation of doppler radar data with a compressible nonhydrostatic model: Oss experiments. Mon. Weather Rev. 133 (7), 1789–1807.
Weisman, M.L., Davis, C., Wang, W., Manning, K.W., Klemp, J.B., 2008. Experiences with 0–36-h explicit convective forecasts with the wrf-arw model. Weather Forecast. 23 (3), 407–437.
Wheatley, D.M., Stensrud, D.J., Dowell, D.C., Yussouf, N., 2012. Application of a wrf mesoscale data assimilation system to springtime severe weather events 2007–09. Mon. Wea. Rev. 140 (5), 1539–1557.
Wheatley, D.M., Yussouf, N., Stensrud, D.J., 2014. Ensemble Kalman Filter Analyses and Forecasts of a Severe Mesoscale Convective System Using Different Choices of Microphysics Schemes. Mon. Wea. Rev. 142 (9).
Wheatley, D.M., Knopfmeier, K.H., Jones, T.A., Creager, G.J., 2015. Storm-scale data assimilation and ensemble forecasting with the nssl experimental warn-on-forecast system. part i: Radar data experiments. Weather Forecast. 30 (6), 1795–1817.
Whitaker, J.S., Hamill, T.M., 2002. Ensemble data assimilation without perturbed observations. Mon. Weather Rev. 130 (7), 1913–1924.
Wilks, D.S., 2011. Statistical Methods in the Atmospheric Sciences. Vol. 100 Academic Press.
Wu, X., Zhang, S., Liu, Z., Rosati, A., Delworth, T., 2013. A study of impact of the geographic dependence of observing system on parameter estimation with an intermediate coupled model. Clim. Dyn. 40 (7–8).
Yussouf, N., Gao, J., Stensrud, D.J., Ge, G., 2013a. The impact of mesoscale environmental uncertainty on the prediction of a tornadic supercell storm using ensemble data assimilation approach. Adv. Meteorol. 2013.
Yussouf, N., Mansell, E.R., Wicker, L.J., Wheatley, D.M., Stensrud, D.J., 2013b. The ensemble Kalman filter analyses and forecasts of the 8 May 2003 Oklahoma city tornadic supercell storm using single- and double-moment microphysics schemes. Mon. Wea. Rev. 141 (10).
Yussouf, N., Dowell, D.C., Wicker, L.J., Knopfmeier, K.H., Wheatley, D.M., 2015. Storm-scale data assimilation and ensemble forecasts for the 27 april 2011 severe weather outbreak in Alabama. Mon. Weather Rev. 143 (8), 3044–3066.
Yussouf, N., Kain, J.S., Clark, A.J., 2016. Short-term probabilistic forecasts of the 31 may 2013 oklahoma tornado and flash flood event using a continuous-update-cycle storm-scale ensemble system. Weather Forecast. 31 (3), 957–983.
Zhang, F., Snyder, C., Sun, J., 2004. Impacts of initial estimate and observation availability on convective-scale data assimilation with an ensemble kalman filter. Mon. Wea. Rev. 132 (5).